Research on Multi-Objective Optimization Power Flow of Power System Based on Improved Remora Optimization Algorithm

Hongyu Long, Zhengxin Chen, Hui Huang*, Linxin Yu, Zonghua Li, Jun Liu and Yi Long

***Abstract*—In this paper, an improved remora optimization algorithm (IROA) is proposed to solve the multi-objective optimal power flow problem (MOOPF). The algorithm introduced the crossover strategy and variance strategy in the differential evolutionary (DE) algorithm. The use of these two strategies can increase the diversity of the remora optimization algorithm (ROA) population and jump out of the defect of being trapped in a local optimum. To better solve the MOOPF, this paper proposed constraint prioritization strategy (CPS), congestion distance ranking strategy (CDRS), and optimal compromise solution strategy (OCSS) to acquire a uniform Pareto optimal set (POS) and the best trade-off solution (BTS). Combined with practical applications, six kinds of objective functions are selected, namely, basic fuel cost, active power loss, emission, voltage deviation, voltage stability, and fuel cost with valve point. The above six objective functions are arranged and combined to obtain the MOOPF problems with dual or triple objectives for solving on IEEE30-bus, IEEE57-bus, and IEEE118-bus systems, which are used to demonstrate the capability of IROA. Furthermore, three performance metrics Hypervolume (HV), Spacing (SP), and Generational Distance (GD) were applied to verify the uniformity and diversity of the POS. The results of the IROA algorithm are compared with those of the non-dominated sorting genetic algorithm II (NSGA-II) and the multi-objective particle swarm optimization algorithm (MOPSO), and it is obtained that the IROA algorithm has a better competitive advantage in solving the MOOPF.**

***Index Terms*—IROA, Pareto front, MOOPF, performance metrics**

Manuscript received March 9, 2023; revised June 26, 2023.

Hongyu Long is a professor level senior engineer of Chongqing Key Laboratory of Complex Systems and Bionic Control, Chongqing University of Posts and Telecommunications, Chongqing 400065, China (e-mail: longhongyu20@163.com).

Zhengxin Chen is a postgraduate student of Chongqing University of Posts and Telecommunications, Chongqing 400065, China (e-mail: zhengxinchen0101@163.com).

Hui Huang is a senior economist of State Grid Chongqing Electric Power Company, Chongqing 400015, China (corresponding author to provide phone: +8613983461967; e-mail: huiwang0226@163.com).

Linxin Yu is a student of Chongqing Electric Power College, Chongqing 400053, China (e-mail: linxinyu111123@163.com).

Zonghua Li is a senior engineer of Chongqing Changan New Energy Vehicles Technology Co., Ltd. (e-mail: zonghuali0305@163.com).

Jun Liu is an engineer of the State Grid Hubei Enshi Power Supply Company, Hubei Enshi, 445000, China (e-mail: junliu_es@163.com).

Yi Long is a senior engineer of the Economic and Technology Research Institute, State Grid Chongqing Electric Power Company, Chongqing 401120, China (e-mail: yilong030500@163.com).

I. Introduction

ELECTRICAL power system is an inseparable system in daily life [1]. The normal life of residents, the orderly development of industrial production, and even the prosperity of the country is inseparable from the safe and stable economic operation of the electrical power system. At the same time, reliability and economy should be considered comprehensively in the planning and operation of power systems to achieve a reasonable balance of investment. The planning of the power system needs to be completed in time and optimized from all possible options. This is a nonlinear problem with multiple constraints, which is difficult to be solved by the traditional derivation method and needs to be solved by systematic engineering methods and advanced intelligent algorithms.

In the early 1960s, the scholar derived the mathematical model of the single objective optimization (OPF) problem [2]. OPF refers to the regulation of relevant input variables such as generator bus voltage, reactive power compensation, generator active power, and the tap ratio of the transformer in the power system to minimize active power loss or fuel cost within the scope permitted by constraints [3-5]. But OPF can only optimize for only one problem [6, 7]. The proposal of MOOPF can be optimized by considering two or more problems, which can better adapt to the increasingly large power system [2, 8-11]. The goals of MOOPF optimization include fuel cost, active power loss, emissions, etc. [12]. MOOPF is a nonlinear and nonconvex problem, it is not possible to use the traditional mathematical model to solve it directly [13]. The only way to solve this problem is to use computer intelligence algorithms [14-18], such as genetic algorithm (GA) [19], differential evolution algorithm (DE) [20], particle swarm optimization algorithm (PSO) [21], whale optimization algorithm (WOA) [22] and so on. However, in daily production, multiple objectives are often optimized at the same time, which leads to conflicts between different objectives. Using intelligent algorithms to solve multi-objective problems, we can find the POS. Therefore, more and more scholars are committed to finding better intelligent algorithms to solve MOOPF. They often use non-dominated sorting genetic algorithm II (NSGA-II) [23], multi-objective particle swarm optimization algorithm (MOPSO) [24] and multi-objective evolutionary algorithm based on decomposition (MODE) [25], modified sine-cosine algorithm [4], improved colliding bodies optimization algorithm [26] , improved bat algorithm [12], firefly algorithm [27], hybrid firefly-bat algorithm [28], slime mould algorithm [29], search group algorithm [30], interior search algorithm [31], marine predators algorithm [32], manta ray foraging algorithm [33] and so on. The outcome indicated that the heuristic algorithm can tackle the MOOPF problem, but there is further room for enhancement.

Remora Optimization Algorithm (ROA) was proposed in 2021 by Heming Jia et al. [34], which mainly simulates the process of Remora attaching to hosts of different body sizes to complete the foraging process. The ROA algorithm is simple in principle and efficient in solving multi-objective problems. To be applied more to the MOOPF problem, we improved the ROA and proposed the IROA. To demonstrate the capability and feasibility of the presented algorithm, IROA tests were executed on three standard power systems (IEEE30-bus, IEEE57-bus, IEEE118-bus). The outcomes indicated that IROA has superior optimization and practicability.

We will organize the remainder of the article according to the following structure: Part II: The math model of MOOPF was established and 3 settlement strategies were presented. Part III: This part introduces the concept, principle and application of ROA algorithm in MOOPF problem. Part IV: This part presents the experimental results and performance analysis of MOOPF using ROA in three standard nodes of power system with different numbers of nodes. Finally, Part V summarizes the work done in this study.

II. MATHEMATICAL MODEL

In practical power system operation, it is necessary to consider optimizing two or more objective functions at the same time. The multi-objective optimization problem can be mathematically formulated as:

$$\min mize Y = (y_1(x,u), y_2(x,u), ..., y_i(x,u)) \tag{1}$$

where, y_1 y_2 and y_i represent the target functions to be minimized, i indicates the amount of optimization goals, and Y is the objective case of optimization.

The constraints of Equation (1) are：

$$D_j(x,u) \geq 0, j = 1,2,...,d \tag{2}$$

$$E_k(x,u) = 0, k = 1,2,...,e \tag{3}$$

in (2) and (3), D_j and E_k indicate the equation constraint and the inequality constraint. e represents the amount of equation restrictions and d indicates the amount of inequality restrictions.

A. Mathematical model of the objective function

In this paper, a total of six objective functions will be considered, including power loss (F_{pl}), fuel cost (F_{cost}), emissions (F_{em}) and fuel cost with valve point effects ($F_{co\text{-}vp}$)., voltage stability (F_{Ld}) and voltage deviation (F_{Vd}).

1) F_{cost}

The objective function for the minimization of the base fuel cost (F_{cost}) is defined as shown in (4) and is expressed in \$/h.

$$F_{cost} = \sum_{i=1}^{N_G}(a_i + b_i P_{Gi} + c_i P_{Gi}^2) \tag{4}$$

where P_{Gi} represents the generator's active power, N_G indicates the quantity of generators, and a_i, b_i, c_i represent the generator fuel cost factors.

2) F_{pl}

The definition of the minimization of the active power loss (F_{pl}) objective function is shown in (5) and is expressed in MW.

$$F_{pl} = \sum_{k=1}^{N_l} c_k \left(|V_i|^2 + |V_j|^2 - 2|V_i||V_j|\cos\delta_{ij} \right) \tag{5}$$

where N_l is the amount of branches in the power system, δ_{ij} is the voltage phase angle difference, V_i represents voltage amplitude and c_k is branch conductance value.

3) F_{em}

The objective function for total exhaust emissions (F_{em}) is defined as shown in (6) and expressed in ton/h.

$$F_{em} = \sum_{i=1}^{N_G}(\alpha_i P_{Gi}^2 + \beta_i P_{Gi} + \gamma_i + \eta_i \exp(\lambda_i P_{Gi})) \tag{6}$$

where, α_i, β_i, γ_i and η_i are the exhaust factors for the i_{th} machine.

4) $F_{co\text{-}vp}$

The equation of the base fuel cost considering the valve point effect ($F_{co\text{-}vp}$) objective function is shown in (7) and has an expression of \$/h.

$$F_{\text{cost\_vp}} = \sum_{i=1}^{N_G}(a_i + b_i P_{Gi} + c_i P_{Gi}^2 + |d_i * \sin(e_i * (P_{Gi}^{\min} - P_{Gi}))|) \tag{7}$$

where, d_i, e_i is the valve point effect fuel factor and P_{Gi}^{min} is the optimum value of active power for the i_{th} machine.

5) F_{Vd}

Voltage deviation (F_{Vd}) is a necessary indicator of the safe and stable operation of system. It can be expressed by the equation(8).

$$F_{Vd} = \sum_{n=1}^{N_{PQ}} | V_n - 1.0 | \tag{8}$$

in(8), F_{Vd} represents the sum of system voltage deviation. N_{PQ} is the number of P-Q nodes of the system.

6) F_{Ld}

The voltage stability index (F_{Ld}) is used to describe the power quality of the power system indicators, the lower the voltage stability index, the smaller the voltage fluctuations. It is shown in equation (9).

$$F_{Ld} = \left| 1 - \sum_{i=1}^{N_v} K_{ji} \frac{V_i}{V_j} \right| \tag{9}$$

$$K_{ji} = -[Y_1]^{-1}[Y_2] \tag{10}$$

where, the number of PV nodes is denoted by N_v, V_i and V_j representing the composite voltage of the ith PV node and the jth PQ node; Y_1, Y_2 are denoting submatrix of the derivative matrix of the network is determined by separating the parameters of PQ nodes and PV nodes.

B. Constraints of the objective function

The MOOPF problem has a strictly constrained minimum optimization. When solving the MOOPF problem, a feasible solution must satisfy all equation and inequality constraints.

1) Equation constraints

The equation constraints include the balance equations for active power and reactive power, expressed in (11) and(12). This means that the active power generated by the generator should be equal to the sum of the active power consumed by the load and the active network losses, while the reactive power generated by the generator should be equal to the sum of the reactive power consumed by the load and the reactive network losses[35].

$$P_{Gi} = P_{Di} + P_{loss} \quad (11)$$

$$Q_{Gi} = Q_{Di} + Q_{loss} \quad (12)$$

where P_{Gi} is the active power emitted by the generator node, P_{Di} is the active power consumed by the load node and P_{loss} is the active power loss on the transmission line, where Q_{Gi} is the reactive power emitted by the generator node, Q_{Di} is the reactive power consumed by the load node and Q_{loss} is the reactive power loss on the transmission line.

2) Inequality constraints

Inequality constraints in the MOOPF problem encompass restrictions on both control variables and state variables.

a) Inequality constraints on control variables

The control variables for the MOOPF problem contain $PVTC$ = [P_G, V_G, T, Q_C], P_G represents the active power emitted by the generator node, V_G is the generator voltage, T is the transformer ratio and Q_C is the reactive power compensation, each control variable requires upper and lower limits:

$$\begin{bmatrix} P_G^{\min} \\ \vdots \\ V_G^{\min} \\ \vdots \\ T^{\min} \\ \vdots \\ Q_C^{\min} \\ \vdots \end{bmatrix} \le \begin{bmatrix} P_G \\ \vdots \\ V_G \\ \vdots \\ T \\ \vdots \\ Q_C \\ \vdots \end{bmatrix} \le \begin{bmatrix} P_G^{\max} \\ \vdots \\ V_G^{\max} \\ \vdots \\ T^{\max} \\ \vdots \\ Q_C^{\max} \\ \vdots \end{bmatrix} \quad (13)$$

As a control variable, it changes as the independent variable changes and can be initialized with a range specification to a valid range. For out-of-bounds control variables, they can be adjusted after each iteration according to equation (14).

$$PVTC_i = \begin{Bmatrix} PVTC_i^{\max}, PVTC_i > PVTC_i^{\max} \\ PVTC_i^{\min}, PVTC_i < PVTC_i^{\min} \end{Bmatrix} \quad (14)$$

where, $PVTC_i^{max}$ is the upper bounds of the control variables and $PVTC_i^{min}$ is the lower bounds of the control variables in group i.

b) Inequality constraints on state variables

The four state variables $PVQS$ = [P_{G1}, V_L, Q_G, S_l] inequality constraints for MOOPF are shown in the following equation(15).

$$\begin{bmatrix} P_G^{\min} \\ \vdots \\ V_L^{\min} \\ \vdots \\ Q_G^{\min} \\ \vdots \\ S_l^{\min} \\ \vdots \end{bmatrix} \le \begin{bmatrix} P_G \\ \vdots \\ V_L \\ \vdots \\ Q_G \\ \vdots \\ S_l \\ \vdots \end{bmatrix} \le \begin{bmatrix} P_G^{\max} \\ \vdots \\ V_L^{\max} \\ \vdots \\ Q_G^{\max} \\ \vdots \\ S_l^{\max} \\ \vdots \end{bmatrix} \quad (15)$$

where P_{G1} is the active power at the balance node, V_L is the voltage at the load node, Q_G is the reactive power from the generator, S_l is the apparent power of the power line.

C. Solution strategy

For multi-objective optimization problems, the optimization process can be more complex because it requires the simultaneous optimization of two or more objective problems. Different constraints must be satisfied simultaneously to overcome the interplay between the determinants of the different problems. After a series of optimization processes, an optimal set of solutions can eventually be obtained rather than a single optimal solution, which requires the decision maker to make trade-offs to obtain the most suitable solution. As a result, Pareto's multi-objective optimization method can be chosen to solve problems related to multi-objective trend optimization.

1) Constraint Prioritization Strategy

Any control variable that violates the inequality constraint during the calculation of the Newton-Raphson method may be adjusted as in equation (14). For state variables a constraint prioritization strategy will be used. When the independent variable is x, formula (16) is used to calculate the total constraint violation.

$$svio(x_i) = \sum_{j \in u} \max(g_p(s, x_i), 0) \quad \mathrm{v} \in P \quad (16)$$

where, v represents the count of inequality constraints.

The constraint prioritization strategy can be described as follows: Randomly select two different solutions in the solution set, denoted as independent variables c_1 and c_2, and calculate their constraint violation quantities $Svio(c_1)$ and $Svio(c_2)$. And the constraint-first Pareto dominance method will be introduced, as in Eq. (17) , when and only when two conditions hold simultaneously, c_1 is said to dominate c_2.

$$\begin{cases} \forall i \in \{1, 2, ..., m\} : f_i(s, c_1) \le f_i(s, c_2) \\ \exists j \in \{1, 2, ..., m\} : f_j(s, c_1) < f_j(s, c_2) \end{cases} \Rightarrow c_1 \prec c_2 \quad (17)$$

The next step is to determine the classification of dominance relationships, which proceeds as follows:

If $Svio(c_1) = Svio(c_2)$, when and only when the equations(17) are satisfied, then c_1 is said to dominate c_2 and is denoted as $c_1 \prec c_2$.

If $Svio(c_1) < Svio(c_2)$, it can be inferred that c_1 will dominate c_2, denoted as $c_2 \prec c_1$.

If $Svio(c_1) > Svio(c_2)$, this indicates that c_2 dominates c_1 and is denoted as $c_2 \prec c_1$.

Finally, if $c_1 \prec c_2$, c_1 will be chosen as the Pareto most compromise optimal solution, if $c_2 \prec c_1$, and c_2 will be chosen as the Pareto most compromise optimal solution.

2) Congestion Distance Ranking Strategy

Congestion distance is a metric describing the degree of crowding between a genetic individual and its neighboring individuals, denoted by i_d. The congestion distance of a population is obtained by making a rectangle enclosing individual i, but not containing other individuals, at the same population level. As shown in Fig. 1.

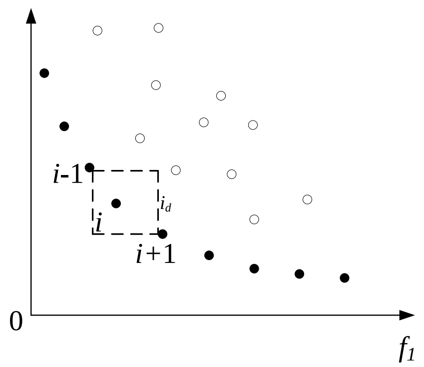

Fig. 1 Congestion Distance Ranking Strategy

From Fig. 1, we can see that the smaller the i_d value, the more other individuals around the individual. Adding congestion distance comparison to the algorithm can make the solved Pareto frontier distribution more competitive, thus ensuring that the number of populations obtained is sufficiently diverse.

3) Optimal compromise solution strategy

Based on the principle of Pareto multi-objective optimization, a Pareto optimal solution set can be obtained after solving the function, but this solution set does not contain a completely optimal solution. Hence, the decision maker needs to choose the most suitable optimal compromise solution based on the existing solution requirements and constraints. To determine whether a solution is an optimal compromise solution, the fuzzy affiliation of this solution can be found using the formula(18).

$$v_k(i)=\begin{cases}1, \ if \quad y_k \le y_k^{\min} \\ \dfrac{y_k^{\max}-y_k}{y_k^{\max}-y_k^{\min}}, \ if \quad y_k^{\min}<y_k<y_k^{\max} \\ 0, \ if \quad y_k \ge y_k^{\max}\end{cases} \tag{18}$$

where, $y_k^{\min}$ is the minimum value of all solution vectors with respect to the objective k, $y_k^{\max}$ is the maximum value of all solution vectors with respect to the objective k.

In solving for the affiliation value, the normalization of a single solution must satisfy a function value that is equal to the sum of the affiliation degrees of all solutions, which can be expressed by the formula(19).

$$v(i)=\frac{\sum_{k=1}^{M} v_k(i)}{\sum_{i=1}^{N}\sum_{k=1}^{M} v_k(i)} \tag{19}$$

In(19), M is the number of unoptimized functions.

From the above, it can be seen that finding an optimal compromise is a matter of finding the option with the maximally non-dominant position in the set of options.

III. Proposed an Improved Remora Optimization Algorithm

A. Remora Optimization Algorithm

Remora Optimization Algorithm (ROA) is a bionic, nature-inspired metaheuristic that simulates the process of remora attaching to hosts of different body sizes and thus completing their foraging. The ROA has now been mathematically simulated for kinetic patterns and kinetic behavior, and its validity has been examined and compared in parallel with ten other natural heuristics. Statistical analysis and comparisons indicate that ROA demonstrates superior application prospects and strong competitiveness when compared to other advanced heuristics. Therefore, it is considered to be applied to the multi-objective optimization of power system tides to obtain better tide results.

1) Principle and process of ROA

Remora is a carnivorous marine fish, often using suction cups to attach to the bottom of a boat or other large fish to swim far and seek food. When there is not enough food around to survive, remora will look for nearby hosts to attach to. Based on the elite idea of the sailfish optimization algorithm, the carp position update equation is as follows (20).

$$X(k+1)=X_{Best}(k)-(rand*(\frac{X_{Best}(k)+X_{rand}(k)}{2})-X_{rand}(k)) \tag{20}$$

k is the number of current iterations, X denotes the individual after position update, X_{rand} denotes the randomly selected individual, and X_{Best} denotes the population's best of individuals before the location update. The formula mainly uses the optimal individual guidance mechanism while adding random selection rules to ensure the search range of the search space.

At the same time, remoras will consider whether it is necessary to change hosts while adsorbing on the current host. Therefore, the fish need to constantly make small movements around the host, which is the adaptive behavior of fish to prevent the host from being attacked and its own safety. This behavior can be expressed by the formula (21)

$$X_{fit}(k+1)=X(k)+(X(k)-X_{pre}(k))*randn \tag{21}$$

where, X_{pre} is represents position of the previous generation. X_{fit} is the fitness value of the current position.

When remora search for a suitable boat bottom or other large fish, they attach themselves to the body of the host for long voyages and search for food in order to save energy while being protected from enemy attacks. The position update in this case is as follow formulas.

$$X(k+1)=Dist*e^{\alpha}*\cos(2\pi\alpha)+X(k) \tag{22}$$

$$\alpha=rand*(a-1)+1 \tag{23}$$

$$a=-\left(1+\frac{k}{K}\right) \tag{24}$$

$$Dist=\left|X_{Best}(k)-X(k)\right| \tag{25}$$

where D_{ist} indicates the distance between the remora and the target prey, k is the current number of iterations; k is the number of current iterations; K is the total number of iterations set; α is a random number in [-1, 1], a is also a random number in [-2, -1].

When remora reach food-rich waters, they detach from their existing hosts and begin the process of localized search for food. The formula for local search is as x

$$X(k+1)=X(k)+A \tag{26}$$

$$A=B*(X(k)-C*X_{Best}(k)) \tag{27}$$

$$B=2V*rand-V \tag{28}$$

$$V=2(1-\frac{k}{K}) \tag{29}$$

where, A is the move step, and its value is related to the current remora fish and dimension. Also, to control the host to remora stature ratio, the parameter C was used to map the remora's position. Assuming that the host volume is 1, the remora is a small fraction of the host volume, and in this paper, we assume that C is a random number of [0, 0.3].

B. Improved remora optimization algorithm

In order to increase the diversity of the population and thus improve the search capability of the algorithm. With more selectivity in the population, the algorithm has a higher probability of finding the optimal compromise solution. Therefore, the crossover strategy and variation strategy of the Differential Evolutionary algorithm (DE) are introduced into the remora optimization algorithm.

1) Variation strategy

This process of remora feeding around the host can be seen as a local search process. The diversity of populations is limited during local search. So, variation strategy is introduced at this point. Adding variation operators to the remora optimization algorithm will increase the population diversity of the algorithm and thus improve its optimization capability. The variation process can be given by the equation(30).

$$X(k+1)=X(k)+\alpha(X_{best}(k)-X(k))+\beta(X(p)-X(q)) \quad (30)$$

In(30), $p\in[1, n]$, $q\in[1, n]$, n is the number of populations; $\alpha\in[0, 1]$, $\beta\in[0, 1]$, which are coefficient of variation.

2) Crossover Strategy

The variation operator increases the search ability while its convergence ability also increases. But on the other hand, it also increases the probability that the algorithm falls into local optimum, at this time, the crossover operation of DE is introduced to increase the number of different gene permutations and combinations on individuals to make the population richer, and different individuals can be selected for the next calculation, so as to avoid the algorithm falling into local optimum. Its calculation formula is as formula (31).

$$X(i)_j=\begin{cases}X(i)_j, rand_{i,j}[0,1]<C_r\\ X(k)_j, k\neq i\end{cases} \quad (31)$$

where $X(i)_j$ denotes the jth value in the ith individual, C_r is the crossover ratio; i, k = 1, 2, …, n; j=1, 2, …, d.

TABLE I
PSEUDO-CODE OF IROA ALGORITHM

Assign initial values for the population size N and the maximum number of iterations T
Initialize positions of the population X_i (i =1, 2, 3, …, N)
Initialize the best solution X_{Best} and corresponding best fitness f (X_{Best})
While k < K do
Calculate the fitness value of each Remora
Check if any search agent goes beyond the search and amend it
Update a, α, V and H
For each Remora indexed by i do
If $H(i)$=0 then
Update the position using Equation(22)
(Evaluate the solutions generated by the global search)
If caught in a local optimum
Updating populations with the variation formula(30)
Updating populations with the variation formula(31)
Else if $H(i)$=1 then
Use equation(20) to update the position
End if
Make a one-step prediction by Equation(21)
Compare fitness values to determine if a host change is needed
If the host is not being replaced, Equation(26) is used as the host feeding mode for Remora
End for
End while
Return X_{Best}

ROA is an algorithm in which the global search is carried out while the local search is carried out. After the process of global-local-global loop, it is able to find the optimal solution set better. Meanwhile the variational and crossover strategies of the differential evolutionary algorithm are added to the ROA algorithm to form an improved ROA algorithm. IROA algorithm is able to increase the variety of individuals during the global search, which makes it easier to find the optimal solution and improve the convergence rate.

3) Pseudocode for IROA

With the above search strategies and formulas, the pseudo-code of IROA algorithm can be written as shown in TABLE I. The flowchart for solving MOOPF problem using the IROA algorithm is displayed in Fig. 6.

IV. SIMULATION RESULTS

Meanwhile, in order to compare the optimization effect of ROA algorithm more intuitively, a total of four algorithms, NSGA-II, PSO algorithm and IROA algorithm, will be used to simulate 11 MOOPF cases under the standard IEEE30 node, standard IEEE57 node test system and standard IEEE118 node test system of power system respectively, and finally the simulation results obtained by the four algorithms will be compared and analyzed.

A. Test Systems

Power system standard test systems have an important role in the research in the field of power systems. The dataset of this test system provides a public research platform for power system planning and operation. The standard test system can provide the basic data for power supply and grid planning, operation optimization modeling and optimization solution methods.

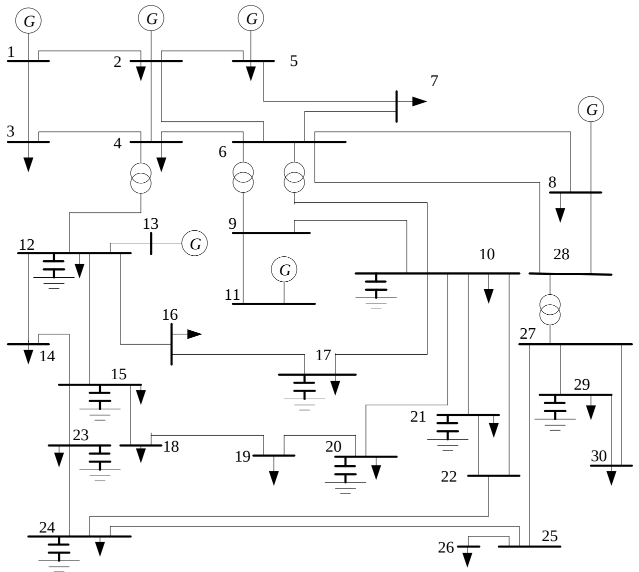

Fig. 2 Power system of IEEE30

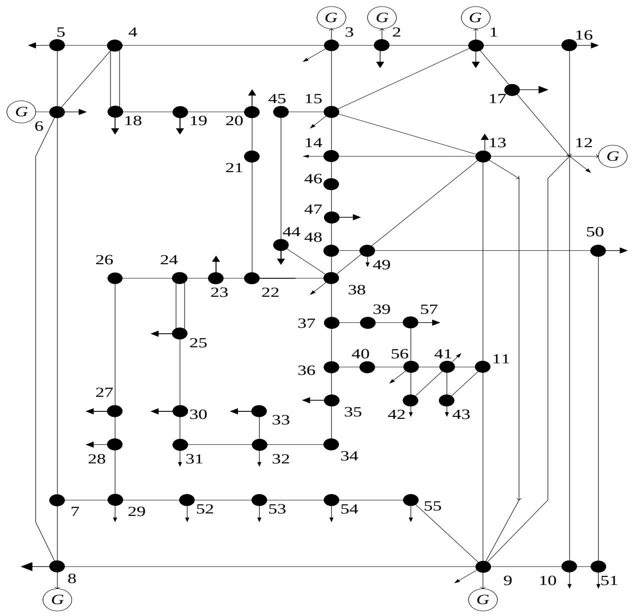

Fig. 3 Power system of IEEE57

As Fig. 2, the IEEE30 node test system has 41 branches, 21 load nodes, 6 generators, 6 reactive power compensation devices and 4 transformers. Nodes 1, 2, 5, 8, 11, and 13 are generator nodes, also known as PV nodes; where node 1 is a balance node.

As Fig. 3, IEEE57 node system, which contains 33 dimensional autotransformers, 7 thermal power generators, 3 reactive power compensators and 17 transformers. 1, 2, 3, 6, 8, 9, and 12 are generator nodes, also called PV nodes; node 1 is the balancing node; P represents the active power of all generators, excluding the balancing node.

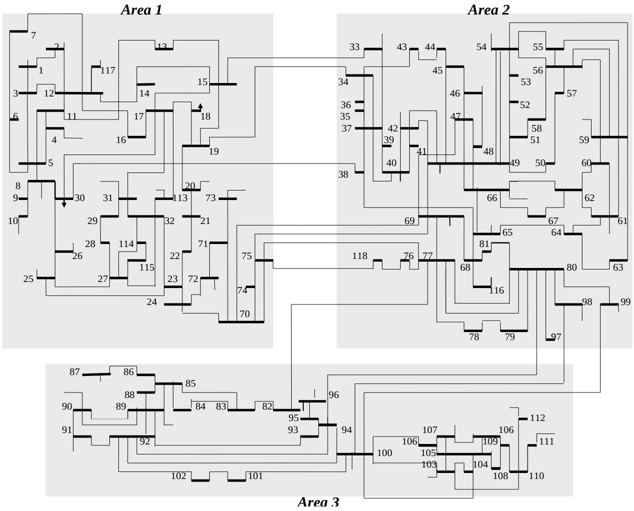

Fig. 4 Power system of IEEE118

As Fig. 4, the IEEE118 node system has 128 independent variables in a 128-dimensional space. The detailed data of the three systems can be found in [27, 37].

In this paper, 8 multi-objective cases will be experimented in the IEEE30 system including 6 bi-objective cases and 2 tri-objective cases, 2 bi-objective cases in the IEEE57 system, and one bi-objective case in the IEEE118 system with the specific objective functions shown in the TABLE II. It should be noted that all simulation experiments in this paper were conducted on MATLAB 2018b software with the following computer information: intel Intel(R) Core (TM) i5-9600k CPU @3.70GHz with 8G RAM.

TABLE II
SIMULATION CASES

Test system	Case No.	F_{Ploss}	$F_{Emission}$	F_{cost}	F_{Vd}	F_{Ld}	$F_{co\text{-}vp}$
IEEE30	1	√		√			
	2		√	√			
	3	√					√
	4	√	√				
	5				√	√	
	6	√			√		
	7	√	√	√			
	8	√	√				√
IEEE57	9		√	√			
	10	√		√			
IEEE118	11		√	√			

B. Algorithm parameter setting

The Pareto Frontier gained for Case 1 is demonstrated in the Fig. 5 for 100, 200, 300, 400, and 500 iterations, respectively, and it can be seen that the output pareto fronts converge well and are uniformly distributed when the iterative number is 300. To save computational time, the iterative number was chosen to be 300. From the literatures, it can be seen that the population sizes selected by scholars in solving the MOOPF problem are all 100 [38-40]. In order to better compare with other literature results, the population number selected in this paper is also 100.

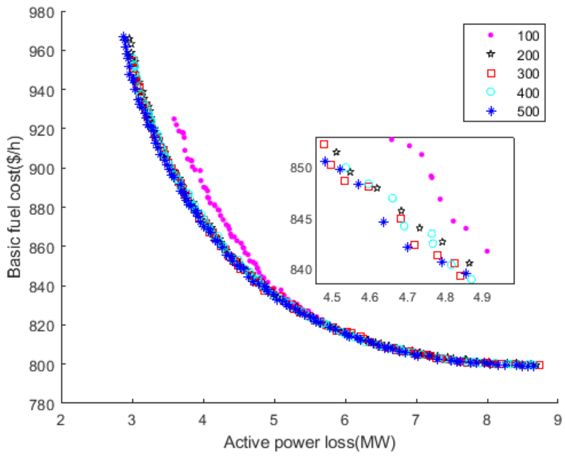

Fig. 5 Number of different iterations of case1

To be able to compare the optimization advantages of the IROA algorithm, two algorithms, MOPSO algorithm and NSGA2 algorithm, were used to do the same experiments for each case in this paper. The algorithms parameter setting of the IROA algorithm, MOPSO algorithm and NSGA2 algorithm are shown in TABLE III.

A. IEEE30 system simulation results

Simulation experiments were completed on IEEE30 system in Case 1 to Case 8.

1) Case1: F_{pl} and F_{cost}

Case 1 will optimize both F_{pl} and F_{cost}. To compare the properties of the IROA, MOPSO and NSGA2 were used to optimize this case.

The acquired results of the tests are shown in TABLE IV, as can be seen from the table, the active power loss obtained by the IROA is **4.9948** MW, and the basic fuel cost is **833.9937** $/h, both of which are better than the MOPSO and the NSGA2. The Pareto Front (PF) is presented in Fig. 7. It can be significantly deduced from the figure the IROA is able to gain a more competitive PF compared to the other two algorithms.

2) Case2: F_{cost} and F_{em}

In Case 2, the two objective functions of F_{cost} and F_{em} are optimized simultaneously. The gained experimental results are summarized in TABLE V. The results of this case demonstrate that the optimal base fuel cost obtained by the IROA algorithm is **831.3102** $/h and the optimal waste emission is **0.2468** ton/h. Compared to the other two algorithms, the optimization results of IROA are better. The PF of the three algorithms is displayed in Fig. 8. Upon observation, the IROA algorithm has improved capabilities in searching the optimal solution and the Pareto solution set has more selectivity. This signifies that the IROA offers a balance between various conflicting objectives.

3) Case3: F_{pl} and $F_{co\text{-}vp}$

Case 3 will optimize both the active power loss and the bi-objective function of the fuel cost considering the valve-electric effect. Three algorithms are used to optimize them separately, and the results are displayed in TABLE VI.

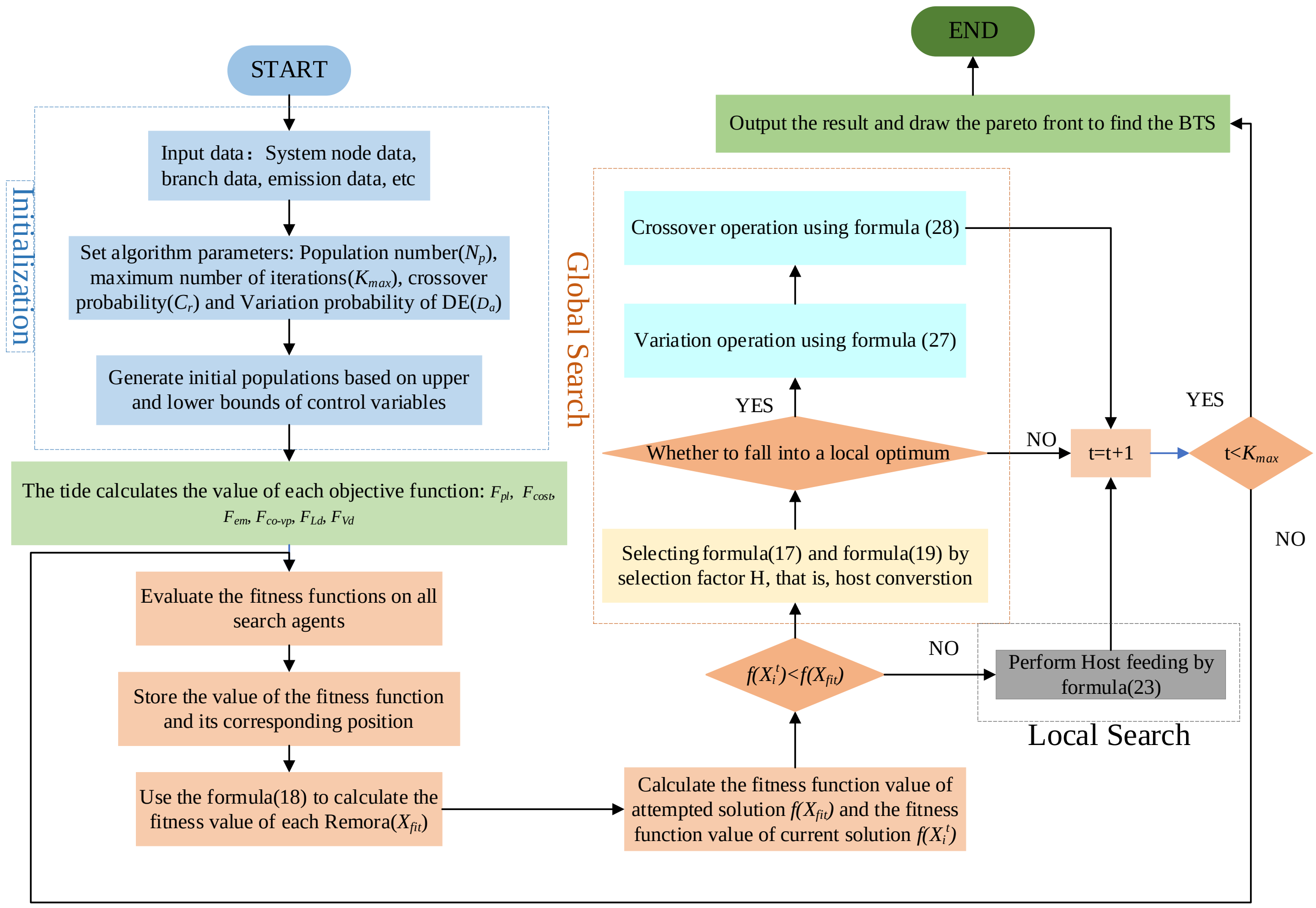

Fig. 6 Flow chart for solving MOOPF problem

TABLE III
PARAMETER SETTINGS FOR THE THREE ALGORITHMS

Algorithms	Parameters	Case1~Case6	Case7~Case8	Case9
IROA	Population size N_p	100	100	100
	Number of iterations K_{max}	300	500	500
	Crossover probability of DE C_r	0.8	0.8	0.8
	Variation probability of DE D_a	0.15	0.15	0.15
MOPSO	Population size N_p	100	100	-
	Number of iterations K_{max}	300	500	-
	Inertia weight factor w_{max}/w_{min}	0.9/0.4	0.9/0.4	-
	Learning factor c_1/c_2	2/2	2/2	-
NSGA2	Population size N_p	100	100	100
	Number of iterations K_{max}	300	500	500
	Mutation index/percentage	20/0.1	20/0.1	20/0.1
	Crossover index/percentage	20/0.1	20/0.1	20/0.1

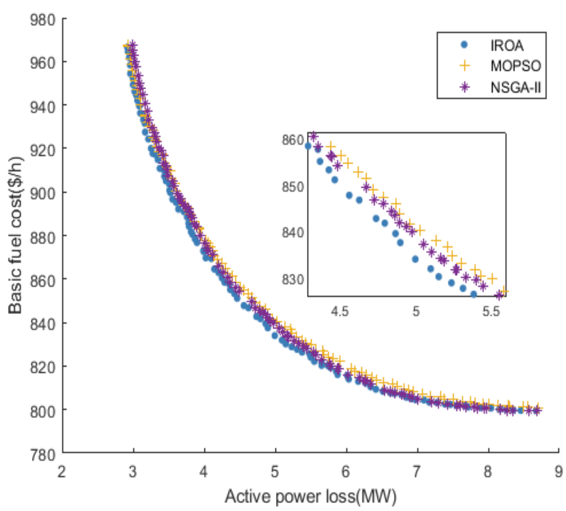

Fig. 7 The pareto front of case1

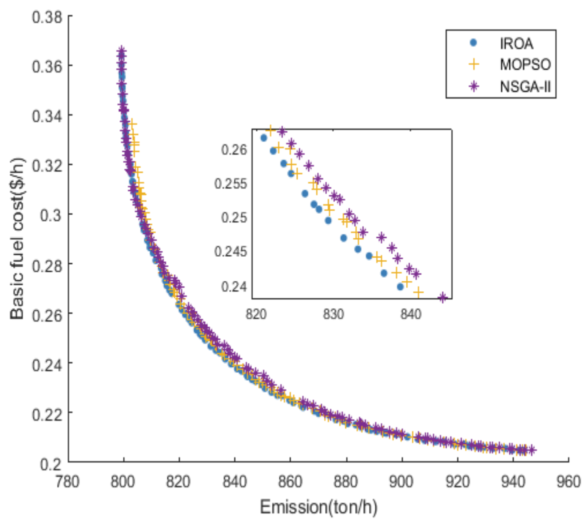

Fig. 8 The pareto front of case2

TABLE IV
THE OPTIMIZATION RESULT OF CASE1

Control Variables (CV)	IROA	NSGA2	MOPSO
P_{G2}(MW)	53.4800	53.0193	51.2690
P_{G5}	32.7025	33.3277	33.1832
P_{G8}	35.0000	34.8352	34.5238
P_{G11}	27.9543	30.0000	29.9987
P_{G13}	21.3902	18.8920	25.5940
V_{G1}(p.u)	1.1000	1.09193	1.1000
V_{G2}	1.0916	1.07825	1.0936
V_{G5}	1.0667	1.05309	1.1000
V_{G8}	1.0787	1.05885	1.0883
V_{G11}	1.0975	1.09925	1.0938
V_{G13}	1.1000	1.09493	1.1000
T_{11}(p.u)	0.1018	0.0748	0.2000
T_{12}	0.0071	0.0872	0.0022
T_{15}	0.0958	0.0891	0.0741
T_{36}	0.0610	0.0805	0.0716
Q_{C10}(p.u)	0.0036	0.0265	0.0500
Q_{C12}	0.0355	0.0346	0.0000
Q_{C15}	0.0249	0.0298	0.0137
Q_{C17}	0.0046	0.0215	0.0424
Q_{C20}	0.0199	0.0138	0.0500
Q_{C21}	0.0465	0.0219	0.0500
Q_{C23}	0.0284	0.0322	0.0500
Q_{C24}	0.0500	0.0458	0.0435
Q_{C29}	0.0300	0.0102	0.0026
$P_{power\ loss}$(MW)	**4.9948**	5.1040	4.9597
$P_{Basic\ fuel\ cost}$($/h)	**833.9937**	835.6152	841.6569

TABLE V
THE OPTIMIZATION RESULT OF CASE2

CV	IROA	NSGA2	MOPSO	MHFPA[38]
P_{G2}(MW)	57.0535	60.2635	59.2282	58.3160
P_{G5}	26.9851	28.8826	27.4519	27.1604
P_{G8}	35.0000	33.3634	35.0000	35.0000
P_{G11}	26.0819	23.9125	25.7069	25.7353
P_{G13}	26.6344	26.0001	26.4458	26.0175
V_{G1}(p.u)	1.0982	1.0414	1.1000	1.1000
V_{G2}	1.0879	1.0239	1.0898	1.0816
V_{G5}	1.0695	0.9923	1.0661	1.0545
V_{G8}	1.0796	1.0105	1.0786	1.0590
V_{G11}	1.0777	1.1000	1.05828	1.0472
V_{G13}	1.1000	1.0516	1.1000	1.0995
T_{11}(p.u)	0.0869	0.1576	0.2000	1.0675
T_{12}	0.0429	0.0086	0.0639	0.9024
T_{15}	0.1275	0.0803	0.1590	0.9902
T_{36}	0.0750	0.0633	0.1209	0.9792
Q_{C10}(p.u)	0.0338	0.0453	0.0000	0.0318
Q_{C12}	0.0477	0.0472	0.0265	0.0085
Q_{C15}	0.0092	0.0269	0.0465	0.0023
Q_{C17}	0.0170	0.0429	0.0500	0.0331
Q_{C20}	0.0256	0.0105	0.0500	0.0500
Q_{C21}	0.0201	0.0430	0.0000	0.0500
Q_{C23}	0.0106	0.0078	0.0500	0.0500
Q_{C24}	0.0500	0.0409	0.0000	0.0243
Q_{C29}	0.0081	0.0211	0.0500	0.0397
$P_{Basic\ fuel\ cost}$($/h)	**831.3102**	833.7782	833.4271	831.6277
$P_{Emission}$(ton/h)	**0.2468**	0.2477	0.2450	0.2468

TABLE VI shows that the optimization results obtained by the IROA algorithm are: the optimal active power loss is **5.6485** MW and the optimal fuel cost with value-point is **865.3990** $/h. IROA and the pareto frontier is shown in Fig. 9. It can be noticed that the Pareto Front obtained after considering the valve point effect is significantly worse than that in case1 without considering the valve point effect. However, the IROA algorithm is still able to draw the pareto front with a competitive advantage over the other two algorithms. Meanwhile, the Pareto front solved by the IROA algorithm makes the distribution of case options more uniform.

4) Case4: F_{pl} and F_{em}

In Case 4, the two objective functions of F_{pl} and F_{em} will be optimized simultaneously, and the simulation outcomes obtained are demonstrated in Fig. 10. In this picture, the PF achieved by the IROA is significantly superior to the MOPSO algorithm and the NSGA2 algorithm, and the distribution of each selectable solution is uniform and smooth. At the same time, the target function's value is displayed in Fig. 10. It is evident that IROA has superior properties in locating the optimal compromise solution, and the optimal active power loss obtained is **2.8853** MW and the emission is **0.2055** ton/h.

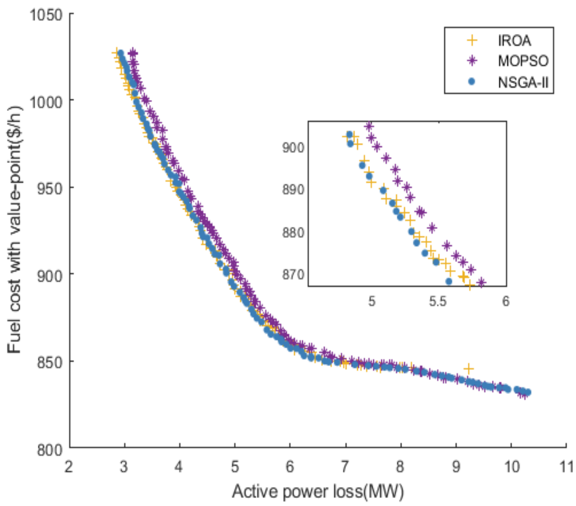

Fig. 9 The pareto front of case3

TABLE VI
THE OPTIMIZATION RESULT OF CASE3

CV	IROA	NSGA2	MOPSO
P_{G2}(MW)	44.4037	39.2881	41.0319
P_{G5}	31.9463	32.8513	33.7751
P_{G8}	34.5046	35.0000	35.0000
P_{G11}	24.1038	27.2908	30.0000
P_{G13}	19.3096	19.4105	15.5671
V_{G1}(p.u)	1.0991	1.0758	1.1000
V_{G2}	1.0897	1.0633	1.0894
V_{G5}	1.0641	1.0361	1.0679
V_{G8}	1.0749	1.0523	1.0777
V_{G11}	1.0951	1.0947	1.1000
V_{G13}	1.0963	1.0963	1.1000
T_{11}(p.u)	0.1304	0.0371	0.2000
T_{12}	0.0294	0.1370	0.0000
T_{15}	0.1123	0.0931	0.1182
T_{36}	0.0880	0.0564	0.0775
Q_{C10}(p.u)	0.0405	0.0152	0.0462
Q_{C12}	0.0147	0.0293	0.0392
Q_{C15}	0.0182	0.0173	0.0489
Q_{C17}	0.0052	0.0216	0.0500
Q_{C20}	0.0354	0.0306	0.0500
Q_{C21}	0.0499	0.0436	0.0500
Q_{C23}	0.0365	0.0377	0.0239
Q_{C24}	0.0288	0.0497	0.0500
Q_{C29}	0.0427	0.0338	0.0242
$P_{Active\ power\ loss}$(MW)	**5.6485**	5.7367	5.3711
$P_{fuel\ cost\ with\ value\text{-}point}$ ($/h)	**865.3990**	871.0438	873.5947

5) Case5: F_{Vd} and F_{Ld}

In Case 5, the two objective functions, F_{Vd} and F_{Ld}, will be solved concurrently, and the resulting results are given in Fig. 11 and TABLE VIII. The figure demonstrates that IROA gains a more competitive PF contrast with other two algorithms. The set of Pareto solutions is evenly distributed and more selectable. In the TABLE VIII, the optimal compromise solution for voltage stability by IROA is **0.4728,** which is improved by 2.23% compared to NSGA2. The voltage deviation solved by IROA is **0.1330**. In conclusion, the solution set and the optimal compromise solution derived by IROA have more competitive advantages over both classical algorithms.

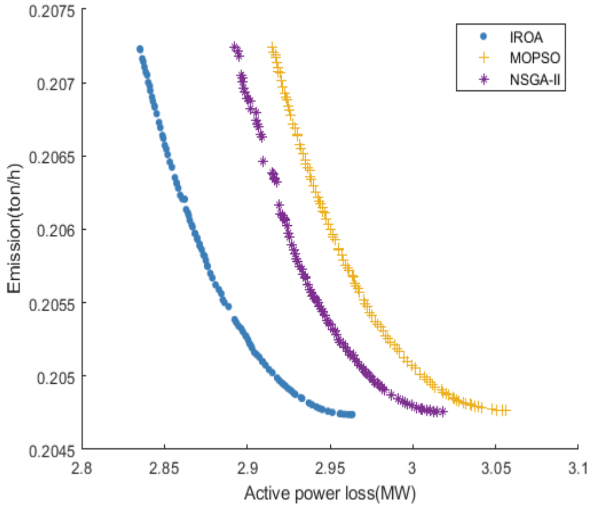

Fig. 10 The pareto front of case4

TABLE VII
THE OPTIMIZATION RESULT OF CASE4

CV	IROA	NSGA2	MOPSO
P_{G2}(MW)	74.5077	74.5478	73.5975
P_{G5}	49.9997	49.9999	50.0000
P_{G8}	34.9999	34.9987	35.0000
P_{G11}	29.9999	29.9986	30.0000
P_{G13}	39.9986	39.9999	40.0000
V_{G1}(p.u)	1.0999	1.0882	1.1000
V_{G2}	1.0965	1.0831	1.1000
V_{G5}	1.0783	1.0628	1.1000
V_{G8}	1.0860	1.0693	1.0936
V_{G11}	1.0999	1.0999	1.1000
V_{G13}	1.0999	1.0999	1.1000
T_{11}	0.0848	0.1266	0.1774
T_{12}	0.0887	0.0017	0.0000
T_{15}	0.0864	0.0617	0.0934
T_{36}	0.0733	0.0554	0.0788
Q_{C10}(p.u)	0.0497	0.0428	0.0500
Q_{C12}	0.0498	0.0100	0.0500
Q_{C15}	0.0402	0.0378	0.0500
Q_{C17}	0.0500	0.0480	0.0500
Q_{C20}	0.0434	0.0311	0.0367
Q_{C21}	0.0499	0.0500	0.0500
Q_{C23}	0.0298	0.0354	0.0222
Q_{C24}	0.0500	0.0488	0.0500
Q_{C29}	0.0215	0.0217	0.0184
$P_{Active\ power\ loss}$ (MW)	**2.8853**	2.9398	2.9789
$P_{Emission}$(ton/h)	**0.2055**	0.2055	0.2053

6) Case6: F_{pl} and F_{Vd}

In Case 6, the two objective functions of F_{pl} and F_{Vd} will be optimized simultaneously, and the obtained simulation results are shown in Fig. 12 and TABLE VI. The minimum active power loss and minimum voltage deviation got by IROA are **3.0712** MW and **0.5265**, which are excellent than the other two algorithms. Meanwhile, the PF solved by IROA is more widely distributed on the coordinate axes, giving more diverse choices to the decision maker.

7) Case7: F_{pl} and F_{em} and F_{cost}

Case 7 will optimize a triple objective function consisting of F_{pl}, F_{em} and F_{cost}. The case will be optimized with three algorithms simultaneously. The experimental data of the objective function is presented in TABLE X.

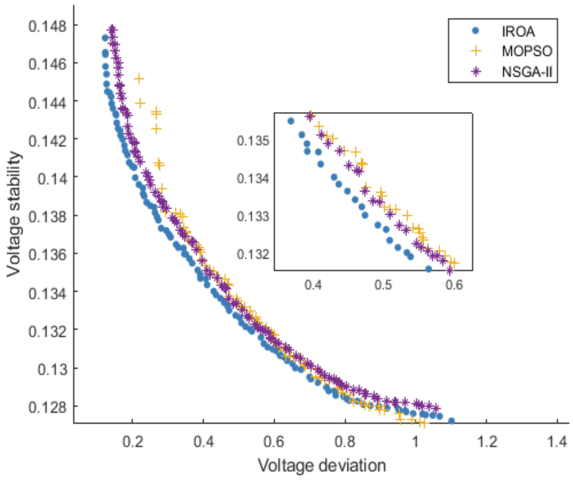

Fig. 11 The pareto front of case5

TABLE VIII
THE OPTIMIZATION RESULT OF CASE5

Control Variables (CV)	IROA	NSGA2	MOPSO
P_{G2}(MW)	27.3805	25.6042	41.7188
P_{G5}	15.0000	41.5439	32.2042
P_{G8}	28.3760	16.2395	35.0000
P_{G11}	18.1403	23.1170	13.5328
P_{G13}	12.2230	28.2348	22.4575
V_{G1}(p.u)	1.0727	1.0614	1.1000
V_{G2}	1.0498	1.0457	1.0649
V_{G5}	0.9795	0.9971	1.0239
V_{G8}	1.0379	1.0280	1.0530
V_{G11}	1.0410	1.0397	1.0816
V_{G13}	1.0307	1.0211	1.0026
T_{11}(p.u)	0.1803	0.0626	0.1527
T_{12}	0.0597	0.1186	0.1342
T_{15}	0.1386	0.1078	0.0896
T_{36}	0.0000	0.0001	0.0000
Q_{C10}(p.u)	0.0397	0.0008	0.0398
Q_{C12}	0.0468	0.0375	0.0043
Q_{C15}	0.0211	0.0172	0.0023
Q_{C17}	0.0399	0.0047	0.0000
Q_{C20}	0.0312	0.0050	0.0372
Q_{C21}	0.0302	0.0302	0.0154
Q_{C23}	0.0276	0.0188	0.0022
Q_{C24}	0.0006	0.0048	0.0500
Q_{C29}	0.0230	0.0498	0.0000
$P_{voltage\ stability}$	**0.4728**	0.4836	0.6340
$P_{voltage\ deviation}$	**0.1330**	0.1334	0.1306

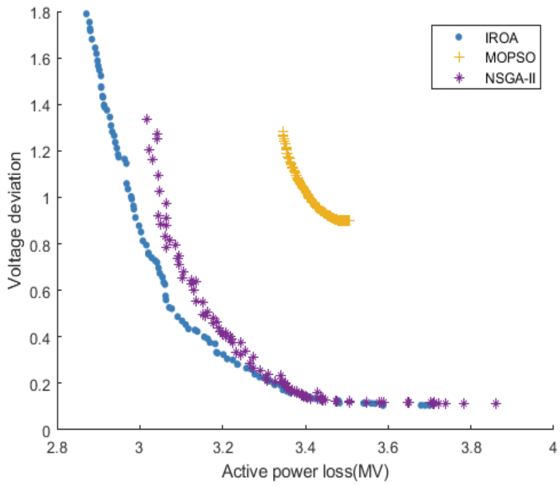

Fig. 12 The pareto front of case6

TABLE X it is obvious that the IROA algorithm obtains better solutions with active power loss of **4.0964** MW; optimal emission of 0.2190 ton/h; and base fuel cost of **877.2487**$/h, respectively, which shows that the IROA algorithm performs equally well in solving the triple objective problem. and the pareto frontier is shown in Fig. 13. The figure shows that the IROA algorithm still performs well in the three-objective optimization problem, again demonstrating the better overall performance of the IROA algorithm.

TABLE IX
THE OPTIMIZATION RESULT OF CASE6

CV	IROA	NSGA2	MOPSO
P_{G2}(MW)	79.9727	80.0000	80.0000
P_{G5}	49.9995	50.0000	50.0000
P_{G8}	35.0000	35.0000	35.0000
P_{G11}	29.9995	30.0000	30.0000
P_{G13}	39.9508	40.0000	40.0000
V_{G1}(p.u)	1.0874	1.0384	1.1000
V_{G2}	1.0825	1.0346	1.1000
V_{G5}	1.0613	1.0146	1.1000
V_{G8}	1.0688	1.0169	1.1000
V_{G11}	1.0448	1.0531	1.1000
V_{G13}	1.0449	1.0247	1.1000
T_{11}(p.u)	0.1911	0.1230	0.2000
T_{12}	0.0717	0.0540	0.2000
T_{15}	0.1677	0.1021	0.1159
T_{36}	0.1274	0.0785	0.1271
Q_{C10}(p.u)	0.0402	0.0084	0.0000
Q_{C12}	0.0020	0.0342	0.0500
Q_{C15}	0.0281	0.0291	0.0000
Q_{C17}	0.0396	0.0099	0.0500
Q_{C20}	0.0203	0.0496	0.0000
Q_{C21}	0.0281	0.0170	0.0311
Q_{C23}	0.0396	0.0275	0.0000
Q_{C24}	0.0489	0.0465	0.0000
Q_{C29}	0.0284	0.0357	0.0000
$P_{Active\ power\ loss}$(MW)	**3.0712**	3.1370	3.4159
$P_{voltage\ deviation}$	**0.5265**	0.5534	0.9809

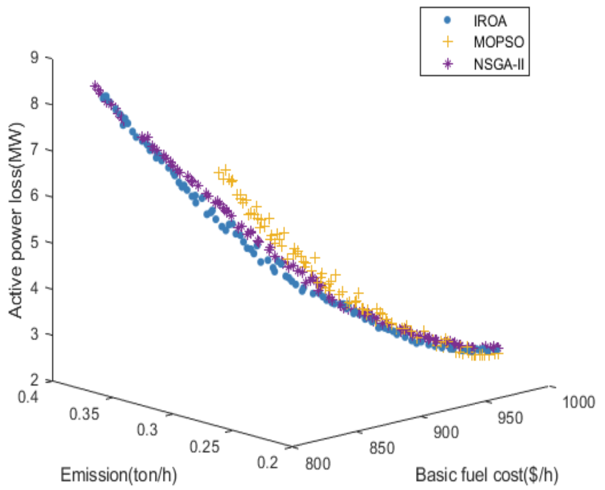

Fig. 13 The pareto front of case7

8) Case8: F_{pl} and F_{em} and $F_{co\text{-}vp}$

Case 8 the optimization process involves simultaneous consideration of three objective functions: F_{em}, F_{pl} and $F_{co\text{-}vp}$, the results of the optimized purpose functions are obtained as shown in TABLE XI. As we have seen, the IROA algorithm still obtains a better optimal compromise solution when faced with a triple objective problem of higher complexity. Its active power loss is **4.4041** MW, the exhaust emissions is **0.2238** ton/h, and the fuel cost considering the valve point effect is **938.4571** $/h. Fig. 14 shows the pareto front obtained after the optimization of three different algorithms. It is evident that the obtained PF distribution becomes less effective as the complexity of the objective function increases, but the IROA algorithm still obtains a more selective solution set, further validating the competitive nature of the algorithm.

TABLE X
THE OPTIMIZATION RESULT OF CASE7

CV	IROA	NSGA2	MOPSO	MOFA-PFA[39]
P_{G2}(MW)	63.4488	58.2342	55.7719	57.8900
P_{G5}	39.3339	38.3757	36.3876	36.2900
P_{G8}	33.9484	34.9999	35.0000	35.0000
P_{G11}	28.3156	29.9406	29.8740	29.2710
P_{G13}	32.8314	38.5710	40.0000	40.0000
V_{G1}(p.u)	1.0978	1.0783	1.1000	1.0985
V_{G2}	1.0891	1.0642	1.0955	1.0869
V_{G5}	1.0674	1.0454	1.0849	1.0625
V_{G8}	1.0707	1.0620	1.0830	1.0767
V_{G11}	1.0807	1.0922	1.1000	1.0857
V_{G13}	1.0642	1.1000	1.0696	1.0386
T_{11}(p.u)	0.0541	0.0931	0.2000	1.0860
T_{12}	0.1829	0.0071	0.0000	0.9930
T_{15}	0.1090	0.1066	0.0584	1.0520
T_{36}	0.0831	0.0554	0.1131	1.0770
Q_{C10}(p.u)	0.0193	0.0226	0.0000	0.0140
Q_{C12}	0.0340	0.0407	0.0000	0.0220
Q_{C15}	0.0309	0.0086	0.0500	0.0080
Q_{C17}	0.0089	0.0082	0.0459	0.0250
Q_{C20}	0.0364	0.0310	0.0500	0.0390
Q_{C21}	0.0281	0.0425	0.0373	0.0270
Q_{C23}	0.0329	0.0193	0.0500	0.0100
Q_{C24}	0.0260	0.0380	0.0500	0.0170
Q_{C29}	0.0349	0.0087	0.0442	0.0500
$P_{Power\ loss}$(MW)	**4.0964**	4.0282	4.0568	4.2179
$P_{Emission}$(ton/h)	**0.2190**	0.2151	0.2169	0.2165
$P_{Basic\ fuel\ cost}$($/h)	**877.2487**	883.9783	878.5838	879.9100

TABLE XI
THE OPTIMIZATION RESULT OF CASE8

CV	IROA	NSGA2	MOPSO
P_{G2}(MW)	58.7071	72.0058	57.0749
P_{G5}	36.5367	35.1946	30.4608
P_{G8}	34.8866	34.3179	35.0000
P_{G11}	28.8529	30.000	30.0000
P_{G13}	31.9603	27.4856	40.0000
V_{G1}(p.u)	1.1000	1.0618	1.1000
V_{G2}	1.0868	1.0547	1.0923
V_{G5}	1.0667	1.0333	1.1000
V_{G8}	1.0727	1.0403	1.0823
V_{G11}	1.0592	1.0220	1.1000
V_{G13}	1.0234	1.0605	1.1000
T_{11}(p.u)	0.2000	0.1083	0.0837
T_{12}	0.1269	0.0683	0.1988
T_{15}	0.1996	0.1099	0.1448
T_{36}	0.1422	0.0875	0.0647
Q_{C10}(p.u)	0.0197	0.0302	0.0500
Q_{C12}	0.0368	0.0012	0.0500
Q_{C15}	0.0420	0.0208	0.0400
Q_{C157}	0.0157	0.0068	0.0500
Q_{C20}	0.0031	0.0189	0.0000
Q_{C21}	0.0212	0.0399	0.0500
Q_{C23}	0.0232	0.0067	0.0500
Q_{C24}	0.0500	0.0241	0.0248
Q_{C29}	0.0128	0.0075	0.0000
$P_{power\ loss}$(MW)	**4.4041**	4.6056	4.6380
$P_{Emission}$(ton/h)	**0.2238**	0.2229	0.2220
$P_{Fuel\ cost\ with\ value\text{-}point}$ ($/h)	**938.4571**	943.2878	941.6254

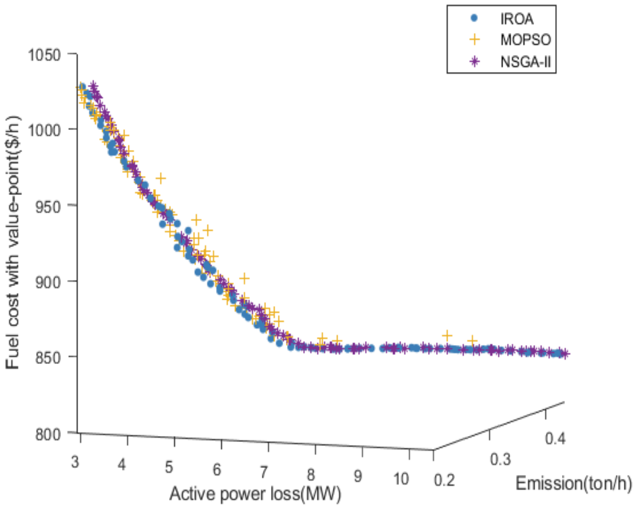

Fig. 14 The pareto front of case8

B. IEEE57 system simulation results

To confirm the effectiveness of the IROA algorithm, two bi-objective optimization experiments were completed on the IEEE57 system. Due to the rise in the system node count, the computational speed is relatively slower and the convergence difficulty of the algorithm increases. The MOPSO algorithm, NSGA2 algorithm was selected to do the same experiments and used to compare the effect of ROA algorithm.

TABLE XII
THE OPTIMIZATION RESULT OF CASE9

CV	IROA	NSGA2	MOPSO	MHFPA[38]
P_{G2}(MW)	100.0000	99.9967	99.6800	100.0000
P_{G3}	84.3158	88.0121	83.4873	85.6281
P_{G6}	100.0000	99.6444	99.3754	99.9643
P_{G8}	342.7495	346.2758	346.9068	342.7870
P_{G9}	99.9548	99.3281	99.9737	99.6791
P_{G12}(p.u)	325.7776	322.4117	327.1706	327.3909
V_{G1}	1.0903	1.0178	1.0627	1.0296
V_{G2}	1.0797	1.0128	1.0487	1.0230
V_{G3}	1.0840	0.9983	1.0089	1.0163
V_{G6}	1.0836	0.9946	0.9808	1.0297
V_{G8}	1.0853	0.9965	0.9708	1.0330
V_{G9}	1.0802	0.9869	0.9766	1.0140
V_{G12}	1.0804	0.9851	0.9739	1.0204
T_{19}	0.0318	0.1086	0.0766	0.9000
T_{20}	0.1470	0.1381	0.0000	1.0974
T_{31}	0.0281	0.1175	0.1882	1.0878
T_{35}	0.0240	0.0851	0.1585	0.9855
T_{36}	0.1167	0.0519	0.0524	1.1000
T_{37}	0.1324	0.1093	0.0916	1.0716
T_{41}	0.1093	0.0878	0.0060	0.9620
T_{46}	0.1105	0.1403	0.1358	1.0112
T_{54}	0.0617	0.0157	0.0571	0.9181
T_{58}	0.0911	0.1030	0.0790	0.9395
T_{59}	0.1163	0.0214	0.0411	0.9060
T_{65}	0.0893	0.1011	0.0435	0.9306
T_{66}	0.0951	0.0178	0.0215	0.9000
T_{71}	0.1374	0.0021	0.0154	0.9529
T_{73}	0.0922	0.1047	0.0788	0.9974
T_{76}	0.1312	0.1064	0.0530	0.9502
T_{80}	0.1439	0.0532	0.1092	0.9333
Q_{C18}(p.u)	0.0920	0.1715	0.1771	0.2106
Q_{C25}	0.0964	0.2409	0.2417	0.1569
Q_{C53}	0.2514	0.0756	0.1396	0.1258
$P_{Basic\ fuel\ cost}$($/h)	**42919.0806**	43074.3556	43035.9109	42939.6926
$P_{Emission}$(ton/h)	**1.3002**	1.3016	1.3202	1.3033

1) Case 9: F_{cost} and F_{em}

Case 9 will optimize both F_{cost} and F_{em} objective functions. The optimization results obtained are shown in TABLE XII. The PF acquired by the 3 methods is depicted in Fig. 15. It can be obviously visualized that the IROA algorithm obtains a preferable compromise. The basic fuel cost is **42919.0806** $/h, and the exhaust emission is **1.3002** ton/h. The pareto front distribution shows the strengths and weaknesses of the three algorithms, and the IROA algorithm gives a more uniform pareto front and a more competitive solution set.

TABLE XIII
THE OPTIMIZATION RESULT OF CASE10

CV	IROA	NSGA2	MOPSO	MOIBA[40]
P_{G2}(MW)	60.1668	45.3010	86.1457	53.4086
P_{G3}	68.0368	74.9928	66.27492	62.6900
P_{G6}	98.8846	89.3289	98.2140	89.8593
P_{G8}	362.5957	367.7005	349.5353	377.9932
P_{G9}	99.9563	99.8887	99.9977	99.9232
P_{G12}(p.u)	410.0000	409.9982	409.85774	410.0000
V_{G1}	1.0608	1.0587	1.1000	1.0536
V_{G2}	1.0574	1.0531	1.1000	1.0467
V_{G3}	1.0545	1.0501	1.1000	1.0436
V_{G6}	1.0689	1.0599	1.1000	1.0521
V_{G8}	1.0736	1.0714	1.1000	1.0613
V_{G9}	1.0670	1.0575	1.1000	1.0481
V_{G12}	1.0557	1.0495	1.1000	1.0337
T_{19}(p.u)	0.1748	0.1475	0.0279	1.0350
T_{20}	0.0622	0.1233	0.2000	0.9496
T_{31}	0.0599	0.0916	0.2000	0.9837
T_{35}	0.0568	0.0338	0.0936	1.0267
T_{36}	0.1345	0.0357	0.0851	1.0055
T_{37}	0.0572	0.0646	0.1590	1.0597
T_{41}	0.0661	0.0631	0.2000	0.9682
T_{46}	0.0264	0.0291	0.0367	0.9558
T_{54}	0.0434	0.1298	0.0362	0.9893
T_{58}	0.0901	0.0916	0.1252	0.9281
T_{59}	0.0833	0.0910	0.2000	0.9192
T_{65}	0.1020	0.1008	0.1408	0.9525
T_{66}	0.0556	0.0663	0.1021	0.9441
T_{71}	0.0683	0.0279	0.1810	0.9527
T_{73}	0.0792	0.0917	0.2000	0.9421
T_{76}	0.0797	0.0642	0.0407	1.0606
T_{80}	0.0674	0.0731	0.1920	0.9688
Q_{C18}(p.u)	0.2544	0.1455	0.0955	0.2343
Q_{C25}	0.1589	0.1119	0.1674	0.1310
Q_{C53}	0.0921	0.1145	0.1607	0.1876
$P_{Basic\ fuel\ cost}$($/h)	**42178.3625**	42313.6702	42242.0330	42098.7213
P_{Ploss}/MW	**10.7071**	10.7751	11.6702	11.4759

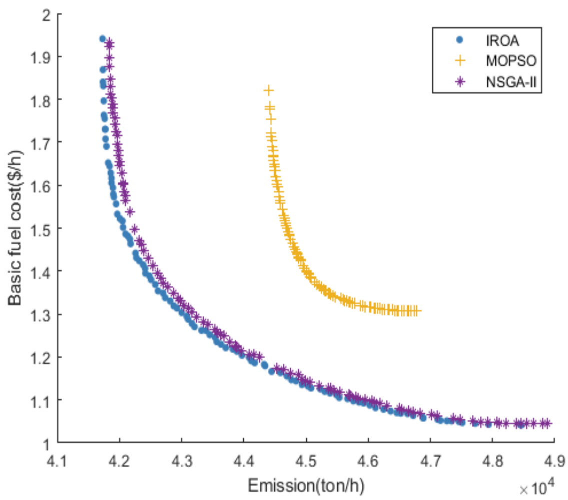

Fig. 15 The pareto front of case9

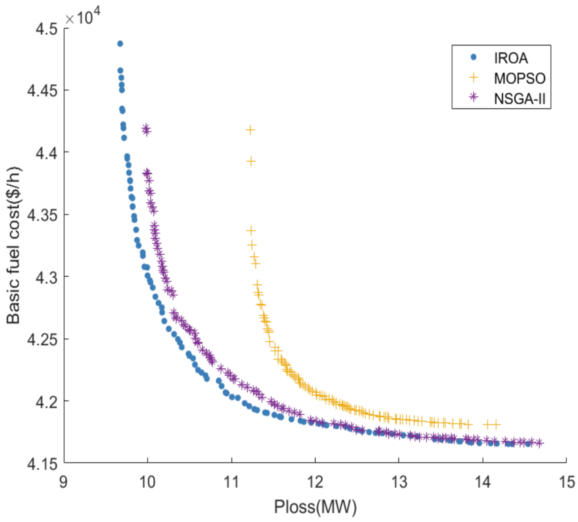

Fig. 16 The pareto front of case10

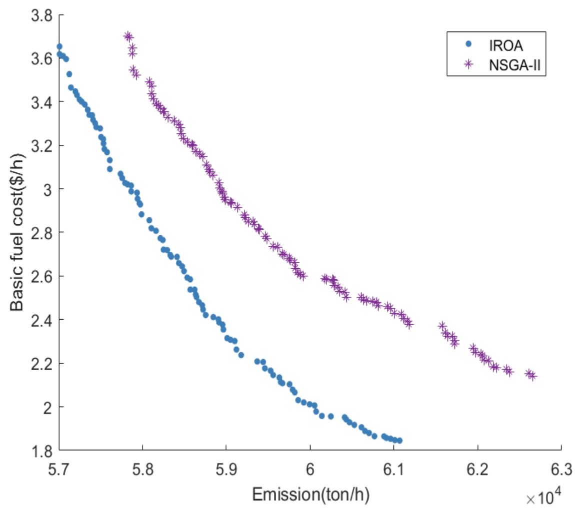

Fig. 17 The pareto front of case11

2) Case10: F_{pl} and F_{cost}

In Case 10, the two target functions, F_{pl} and F_{cost}, will be optimized concurrently, and the optimization values obtained are indicated in TABLE XIII. After the optimization of the IROA algorithm, the value of the basic fuel cost is **42178.3625** \$/h and the value of the active power loss is **10.7071** MW. In comparison with the other two methods, IROA has greater efficiency in finding the optimal compromise solution. Also, the PF acquired by the three algorithms is shown in Fig. 16. It becomes evident that the distribution of the solution set obtained by IROA is more global, allowing more choices for the decision maker. As opposed to the other two algorithms, the IROA has better distributivity and more uniform distribution. This is enough to see that the IROA algorithm has better results in finding the optimal solution of MOOPF.

C. IEEE118 system simulation results

1) Case11: F_{cost} and F_{em}

In Case 11, both F_{cost} and F_{em} objective functions will be optimized simultaneously. Since the MOPSO algorithm cannot converge when calculated on the IEEE118 system, the ROA algorithm and the NSGA2 algorithm are used to optimize it, and the obtained 128-dimensional independent variable optimization results and the values of the optimal object function are provided in TABLE XIV. It becomes evident that the BTS obtained by IROA is the specific values of the basic fuel cost is **58753.6039** \$/h and the value of the emissions is **2.4210** ton/h.

Fig. 17 visually depicts the Pareto frontier produced by applying the two algorithms. We can clearly see that the computational complexity increases as the dimensionality of the independent variables increases, resulting in the Pareto front obtained by this algorithm being inferior to the IEEE30 and IEEE57 system. However, in the figure, the difference between the IROA and NSGA2 algorithms can still be seen, and IROA still obtains a more competitive pareto front. The above experiments are sufficient to see that the IROA algorithm has a better performance in both seeking the optimal solution and drawing the PF.

D. Performance Evaluation

From the aforesaid test outcomes, it can be concluded that the IROA algorithm can acquire a more superior optimal compromise and pareto fronts compared to the MOPSO algorithm and NSGA-II algorithm. In order to compare the advantages of ROA algorithm more intuitively, three performance metrics include Hypervolume (HV), Spacing (SP), and Generational Distance (GD), which are selected in this paper to evaluate the diversity, uniformity of pareto solution set, and convergence of algorithms, respectively.

In this paper, the HV, SP, and GD metrics are calculated for these six cases based on the Pareto solution sets obtained from three algorithms, IROA, MOPSO, and NSGA-II, on the IEEE30 system with four dual-objectives and two triple-objectives. It is worth stating that for each algorithm, for each case, 20 independent iterations were performed, with 300 iterations for each experiment.

1) HV

The HV index was proposed by Zitzler et al [43]. It is applied to weigh the volume of a target space in which there exists at least one space occupied by a non-occupying collection of solutions. HV index is a good measure of the diversity and convergence of the algorithm. A higher HV index signifies that the solution set exhibits enhanced convergence and diversity, thereby approaching the true Pareto frontier. As a result, it represents a superior collection of non-dominated solutions. It is calculated as (32)

$$HV = \delta(\bigcup_{i=1}^{|S|} v_i) \tag{32}$$

where, δ denotes the Lebesgue measure, used for volume measurement; $|S|$ represents the count of non-dominated solution sets, and v_i represents the hypervolume consisting of the reference point and the ith solution within the solution set.

2) SP

SP refers to the quantified smallest standard deviation of the distance between every single solver and other solvers. A smaller SP value indicates a more homogeneous set of Pareto solutions.

$$SP = \sqrt{\frac{1}{|P|-1}\sum_{i=1}^{|P|}(\bar{d}-d_i)^2} \tag{33}$$

where, P denotes the entire pareto front; di denotes the ith solution in the solution set; and $\vec{d}$ denotes the mean value of

TABLE XIV
THE OPTIMIZATION RESULT OF CASE11

CV	IROA	NSGA2	Control variables	IROA	NSGA2
P_{G4}(MW)	5.0000	10.6402	V_{G26}	0.9868	0.9924
P_{G6}	6.6419	16.5024	V_{G27}	0.9423	0.9338
P_{G8}	6.2206	6.2025	V_{G31}	1.0199	1.0100
P_{G10}	249.6831	254.5999	V_{G32}	0.9811	1.0186
P_{G12}	276.4132	207.1168	V_{G34}	0.9833	0.9965
P_{G15}	10.8777	13.1936	V_{G36}	0.9896	0.9995
P_{G18}	53.3815	67.7711	V_{G40}	1.0485	1.0388
P_{G19}	5.8105	6.7298	V_{G42}	1.0630	1.0626
P_{G24}	5.0000	10.5524	V_{G46}	1.0534	1.0430
P_{G25}	100.0000	100.0000	V_{G49}	0.9960	1.0269
P_{G26}	102.9708	101.0980	V_{G54}	0.9955	1.0495
P_{G27}	8.6017	8.7462	V_{G55}	0.9915	1.0344
P_{G31}	10.3170	10.1454	V_{G56}	1.0270	1.04370
P_{G32}	54.1897	43.5886	V_{G59}	1.0554	1.0032
P_{G34}	8.7623	8.1147	V_{G61}	1.0473	1.0224
P_{G36}	25.0000	25.4320	V_{G62}	1.0199	0.9916
P_{G40}	8.7920	8.0573	V_{G65}	1.0579	1.0010
P_{G42}	9.4605	8.0003	V_{G66}	1.0562	1.0416
P_{G46}	56.1314	75.8906	V_{G69}	1.0118	1.0663
P_{G49}	250.0000	247.0330	V_{G70}	1.0430	0.9552
P_{G54}	152.9166	76.6452	V_{G72}	1.0043	1.0293
P_{G55}	25.0000	38.9495	V_{G73}	0.9965	1.0302
P_{G56}	27.7466	25.7784	V_{G74}	0.9934	1.0029
P_{G59}	57.1411	132.8590	V_{G76}	1.0119	1.0550
P_{G61}	200.0000	193.5529	V_{G77}	1.0154	1.0772
P_{G62}	25.0000	30.8124	V_{G80}	1.0047	1.0040
P_{G65}	420.0000	341.4283	V_{G85}	1.0038	0.9663
P_{G66}	241.6464	303.6128	V_{G87}	0.9733	0.9769
P_{G69}	30.2945	49.7666	V_{G89}	1.0303	1.0494
P_{G70}	10.0000	14.0931	V_{G90}	0.9794	1.0155
P_{G72}	5.0000	5.8220	V_{G91}	1.0262	1.0252
P_{G73}	5.0025	5.6324	V_{G92}	1.0318	1.0776
P_{G74}	39.4420	29.4916	V_{G99}	1.0242	1.0546
P_{G76}	31.1341	25.0343	V_{G100}	1.0307	1.0583
P_{G77}	176.0161	197.4512	V_{G103}	1.0330	1.0171
P_{G80}	25.0000	35.5182	V_{G104}	1.0428	0.9814
P_{G85}	10.0000	10.0000	V_{G105}	1.0246	0.9884
P_{G87}	184.3840	140.4687	V_{G107}	1.0106	1.0475
P_{G89}	118.9866	71.8654	V_{G110}	1.0208	1.0099
P_{G90}	8.0000	9.7378	V_{G111}	1.0421	1.0223
P_{G91}	20.9944	23.0993	V_{G112}	1.0080	1.0083
P_{G92}	179.1091	101.1477	V_{G113}	1.0012	1.0144
P_{G99}	116.7986	144.6727	V_{G116}	1.0017	0.9880
P_{G100}	132.2775	207.6204	T_{54}(p.u)	0.0460	0.0355
P_{G103}	8.0000	8.2211	T_{58}	0.0763	0.1039
P_{G104}	31.0139	25.0519	T_{59}	0.0829	0.0741
P_{G105}	26.9262	49.8663	T_{65}	0.0739	0.1004
P_{G107}	9.1367	17.6540	T_{66}	0.0730	0.0171
P_{G110}	25.6514	25.1645	T_{71}	0.0576	0.0774
P_{G111}	31.9422	54.5549	T_{73}	0.0290	0.1993
P_{G112}	32.4938	42.7042	T_{76}	0.0352	0.0621
P_{G113}	40.0202	41.0419	T_{80}	0.0346	0.1161
P_{G116}	31.7032	30.9885	Q_{C18}(p.u)	0.01717	0.2155
V_{G1}(p.u)	1.0470	1.0270	Q_{C25}	0.0249	0.1680
V_{G4}	1.07020	1.0445	Q_{C53}	0.2344	0.0369
V_{G6}	1.0115	0.9604	Q_{C18}	0.1856	0.1465
V_{G8}	0.9857	1.0265	Q_{C18}	0.1108	0.0117
V_{G10}	1.0364	1.0221	Q_{C25}	0.2176	0.1739
V_{G12}	0.9856	1.0230	Q_{C53}	0.0382	0.1758
V_{G15}	0.9812	1.0173	Q_{C18}	0.2446	0.0932
V_{G18}	0.9711	1.0055	Q_{C18}	0.1476	0.2951
V_{G19}	1.0428	0.9733	Q_{C25}	0.1636	0.1581
V_{G24}	1.0548	1.0577	Q_{C53}	0.2528	0.0267
V_{G25}	0.9895	0.9988	Q_{C18}	0.2290	0.1737
			$P_{Basic\ fuel\ cost}$($/h)	**58753.6039**	59879.6818
			$P_{Emission}$(ton/h)	**2.4210**	2.6056

all d_i. It is worth noting that the *SP* index only measures the uniformity of the solution set without considering its extensiveness. When *SP* = 0, it signifies that there exists equidistance between the solutions of this solution set.

3) GD

GD denotes the smallest mean separation of each point in the solved subset from the true solution set, and a lower value of GD means better convergence. GD index can be expressed by the formula (34).

$$GD = \frac{\sqrt{\sum_{y \in P} x_{\min} \times dis(x, y)^2}}{|P|} \quad (34)$$

where P represents the collection of solutions found by the method, P^* is a set of homogeneously spaced points of reference suspended from the PF sampling; $dis\,(x, y)$ denotes the Euclidean distance between point y in the solution set P and point x in the reference set P^*.

4) Results of performance indicators

It is worth mentioning that box plots are made for the analysis of HV, SP and GD indexes in this paper. A box plot is a statistical chart used to show the dispersion of the data. It shows the maximum value, minimum value, median and two quartiles of the obtained optimal solution set, which can visualize the distribution of a set of data.

TABLE XV
DETAILED DATA OF THE BOXES

Index	Cases	IROA		MOPSO		NSGA2	
		Mean	Deviation	Mean	Deviation	Mean	Deviation
SP	Case 1	0.9176	0.1902	1.1537	1.4558	0.8831	0.0950
	Case 2	0.8583	0.0687	1.7496	2.9594	0.8381	0.0525
	Case 3	0.9507	0.0534	1.6335	3.4559	1.0234	0.0860
	Case 4	0.0012	0.0004	0.0020	0.0076	0.0001	0.0007
	Case 7	1.1171	0.0905	1.4984	3.1001	1.0958	0. 0995
	Case 8	0.0190	0.0094	0.1050	0.1249	0.0070	0.0015
HV	Case 1	896.2558	21.6534	526.2380	276.9425	869.2816	29.2753
	Case 2	21.1400	0.3522	11.8351	7.5588	24.1643	0.2930
	Case 3	1244.8415	12.6642	693.0386	469.3449	1210.4582	33.7775
	Case 4	0.0013	0.0001	0.0003	0.0003	0.0012	0.0003
	Case 7	0.5798	0.0109	0.9168	0.2225	0.5837	0.0234
	Case 8	11.8264	0.6690	8.6911	2.1880	11.8753	0.1298
GD	Case 1	0.0675	0.0157	0.0797	0.0196	0.2497	0.1018
	Case 2	0.0642	0.0150	0.3380	0.2235	0.0644	0.0149
	Case 3	0.0731	0.0169	0.0930	0.0224	0.0821	0.0295
	Case 4	0.0056	0.0022	0.0210	0.0165	0.0156	0.0135
	Case 7	0.0737	0.0172	0.2545	0.2534	0.0888	0.0212
	Case 8	0.0197	0.0077	0.0330	0.0166	0.0320	0.0108

TABLE XVI
AVERAGE OPTIMIZATION TIME

Algorithms	Average optimization time (second)										
	Case 1	Case 2	Case 3	Case 4	Case 5	Case 6	Case 7	Case 8	Case 9	Case 10	Case 11
IROA	141.689	136.704	141.053	149.195	139.207	140.193	152.198	149.990	345.303	339.225	1084.825
NSGA2	147.961	141.384	148.511	158.723	153.680	139.574	161.535	153.670	354.888	353.493	1235.293
MOPSO	156.294	151.089	161.137	166.990	239.120	144.496	166.524	155.970	362.650	366.825	-

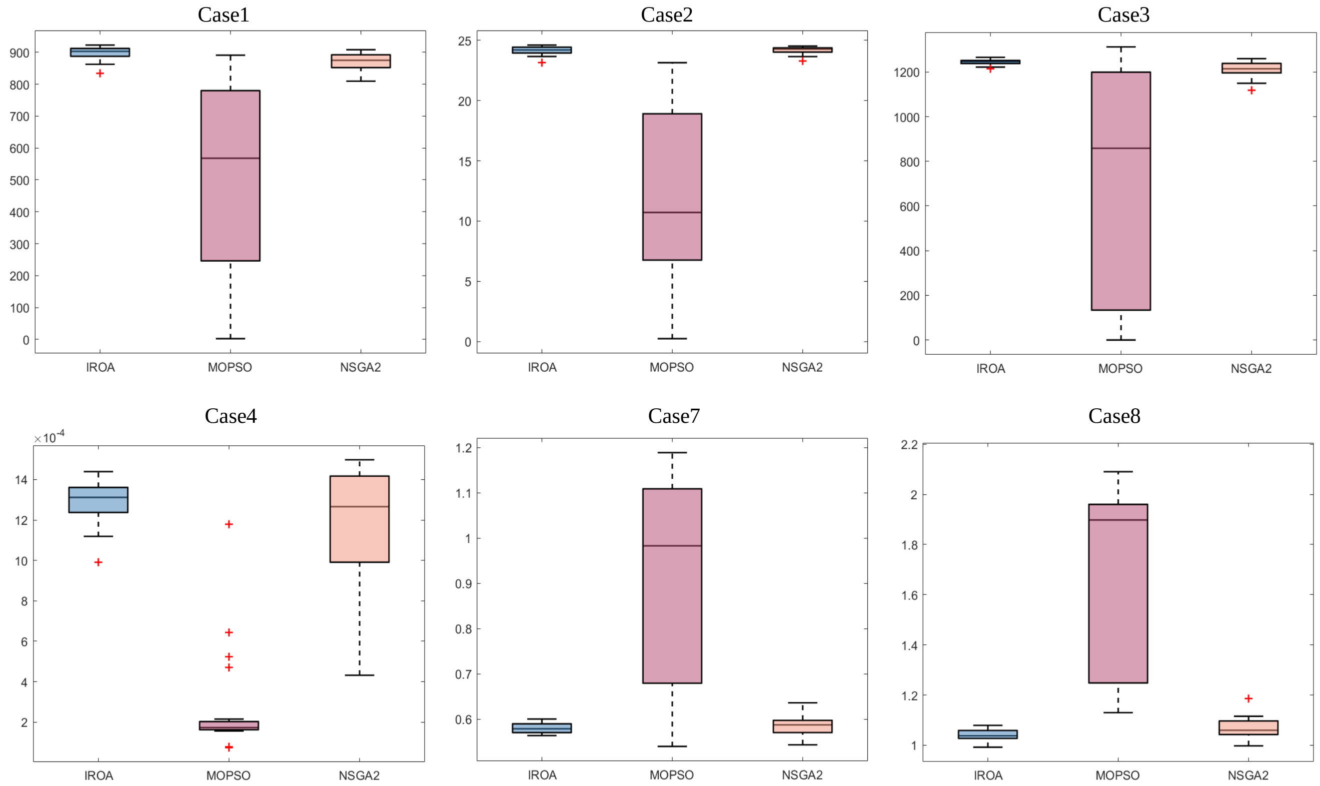

Fig. 18 Plot box of HV

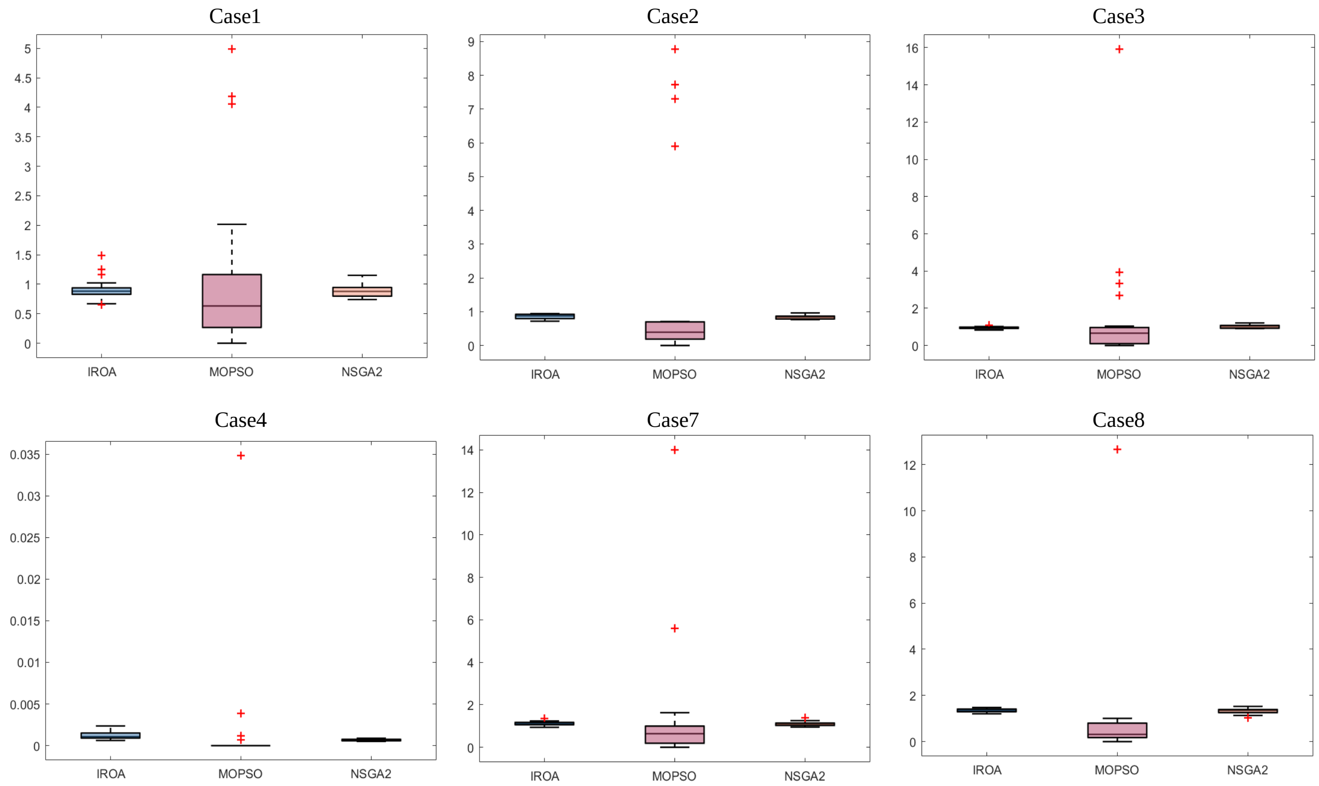

Fig. 19 Plot box of SP

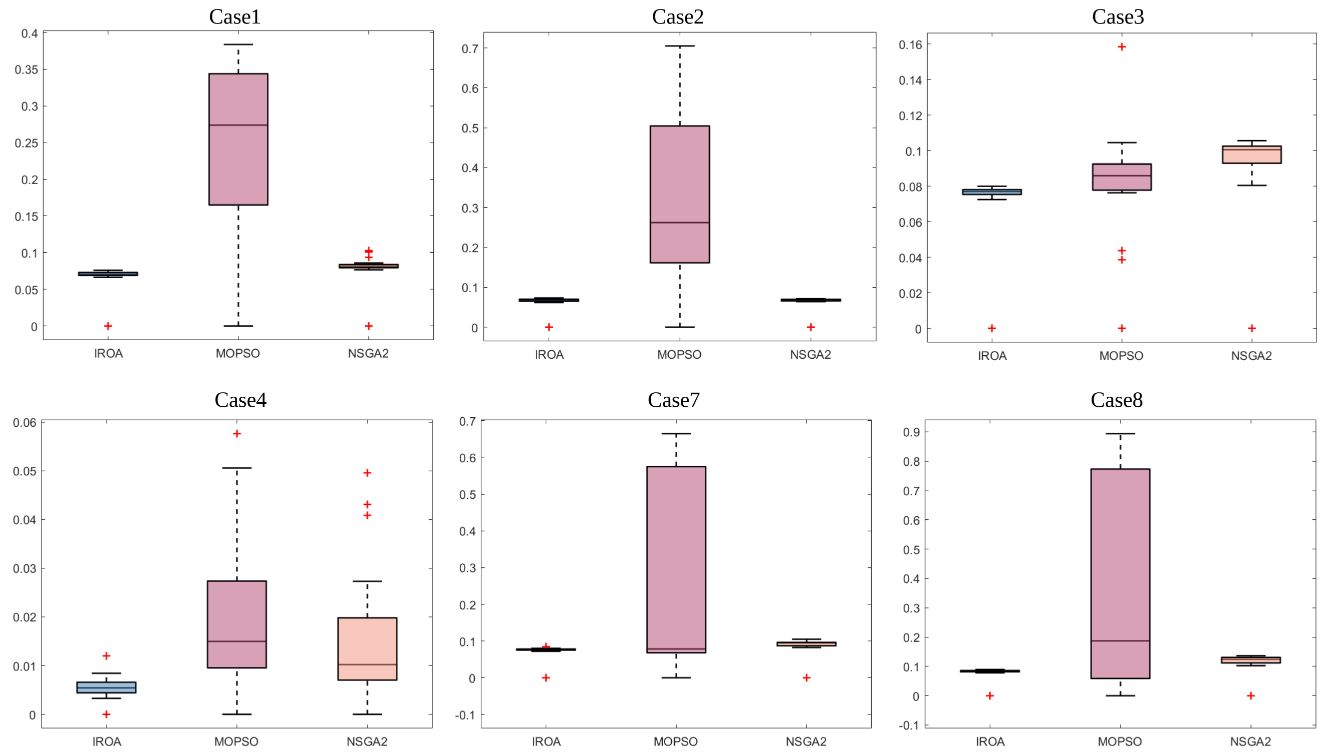

Fig. 20 Plot box of GD

In Fig. 18, the box plot of HV index of case1-case4 and case7-case8 is shown. Each vignette contains three different algorithms, which are IROA, MOPSO, and NSGA2 algorithms. It is obvious to see that from case1-case4, the convergence and diversity of the IROA algorithm perform optimally compared to the MOPSO algorithm and the NSGA-II algorithm. In case7 and case8, the performance is worse, but it can be seen that the IROA algorithm has stability in every calculation compared to the MOPSO algorithm, and 20 independent repetitions of the experiment are able to obtain similar optimal solution sets.

In Fig. 19, the box plot of SP index of case1-case4 and case7-case8 is shown. From the figure, it is clear that the IROA algorithm obtains more uniform solution sets than MOPSO algorithm and NSGA-II algorithm in computing case1, case2, case3, case7 and case8. And the solution sets obtained by the IROA algorithm are stable for each experiment, unlike the MOPSO algorithm, where the calculation results are extremely unstable with large gaps.

In Fig. 20, the box plot of GD index of case1-case4 and case7-case8 is shown. The convergence of the three algorithms is clearly illustrated in the figure. The value of

DG closer to 0, it can be determined that the convergence value of the algorithm is better. According all the cases, the convergence of the solution set obtained by the IROA algorithm is better than that of the other two algorithms. Also, by comparing the lengths of the square boxes, it can be seen that the stability of the IROA algorithm is better than that of the MOPSO algorithm and the NSGA-II algorithm.

At the same time,

TABLE XV reveals the assessment results in detail for SP, HV and GD. In summary, the results of 20 independent replications demonstrate that the convergence, extensiveness, and uniformity of solution set distribution of the IROA algorithm in solving the MOOPF problem are better than those of the MOPSO and NSGA-II algorithms.

E. Algorithm Complexity

In practical engineering problems, power system scheduling departments tend to take the least amount of time to make decisions. In this paper, the time complexity is chosen to evaluate how fast each algorithm gets the results. The TABLE XVI shows the time required to solve case 1-11 for three algorithms (IROA algorithm, MOPSO algorithm and NSGA2 algorithm), each containing 20 independent repetitions of the experiment. It can be concluded that the IROA algorithm has a faster search speed compared to MOPSO and NSGA2, efficiency of the IROA algorithm is further validated.

V. CONCLUSION

In this paper, an IROA algorithm proposed for nonlinear nonconvex MOOPF Problems by using crossover strategy and mutation strategy in DE algorithm. The introduction of these two strategies makes the population of IROA more diverse and avoids the algorithm falling into local optimum. Three Strategies, CPS, CDRS and OCSS, are proposed to obtain POS in IROA. The POS distribution is uniform and can satisfy all the constraints of MOOPF. The solution ability of IROA is tested on IEEE30-bus, IEEE57-bus and IEEE118-bus standard systems. Six objective functions of F_{pl}, F_{cost}, F_{em}, $F_{co\text{-}vp}$, F_{Ld}, F_{Vd} are selected, and the multi-objective problem composed of these four objective functions is solved. The experimental results verify the superiority and generality of IROA algorithm. HV, SP and GD are used to evaluate the uniformity, diversity and proximity of POS distribution obtained by IROA algorithm. It is proved that IROA is better than NSGA-II and MOPSO, not only the POS is more uniform, but also the BTS is better. Therefore, the IROA algorithm proposed in this paper has a better competitive advantage in solving MOOPF problem, and can effectively solve the actual power system MOOPF problem.

REFERENCES:

[1] D. Urgun, C. Singh, V. Vittal, "Importance sampling using multilabel radial basis classification for composite power system reliability evaluation," *IEEE Systems Journal*, vol. 14, no. 2, pp. 2791-2800, 2020.

[2] E. Naderi, M. Pourakbari-Kasmaei and H. Abdi, "An efficient particle swarm optimization algorithm to solve optimal power flow problem integrated with FACTS devices," *Applied Soft Computing*, vol. 80, pp. 243-262, 2019.

[3] K. Nusair, F. Alasali, A. Hayajneh, and W. Holderbaum, "Optimal placement of FACTS devices and power-flow solutions for a power network system integrated with stochastic renewable energy resources using new metaheuristic optimization techniques," *International Journal of Energy Research*, vol. 45, no. 13, pp. 18786-18809, 2021.

[4] A. Attia, R. A. El Sehiemy and H. M. Hasanien, "Optimal power flow solution in power systems using a novel sine-cosine algorithm," *International Journal of Electrical Power & Energy Systems*, vol. 99, pp. 331-343, 2018.

[5] S. I. Evangeline and P. Rathika, "Wind farm incorporated optimal power flow solutions through multi-objective horse herd optimization with a novel constraint handling technique," *Expert Systems with Applications*, vol. 194, 2022.

[6] M. E. Cimen, Z. B. Garip and A. F. Boz, "Chaotic flower pollination algorithm based optimal PID controller design for a buck converter," *Analog Integrated Circuits and Signal Processing*, vol. 107, no. 2, pp. 281-298, 2021.

[7] S. Abd El-Sattar, S. Kamel, R. A. El Sehiemy, F. Jurado, and J. Yu, "Single- and multi-objective optimal power flow frameworks using Jaya optimization technique," *Neural Computing & Applications*, vol. 31, no. 12, pp. 8787-8806, 2019.

[8] R. H. Liang, C. Y. Wu, Y. T. Chen, and W. T. Tseng, "Multi-objective dynamic optimal power flow using improved artificial bee colony algorithm based on Pareto optimization," *International Transactions on Electrical Energy Systems*, vol. 26, no. 4, pp. 692-712, 2016.

[9] M. Ghasemi, S. Ghavidel, M. M. Ghanbarian, M. Gharibzadeh, and A. A. Vahed, "Multi-objective optimal power flow considering the cost, emission, voltage deviation and power losses using multi-objective modified imperialist competitive algorithm," *Energy*, vol. 78, pp. 276-289, 2014.

[10] S. B. Pandya, S. Ravichandran, P. Manoharan, P. Jangir, H. H. Alhelou, "Multi-objective optimization framework for optimal power flow problem of hybrid power systems considering security constraints," *IEEE Access*, vol. 10, pp. 103509-103528, 2022.

[11] A. Khan, H. Hizam, N. I. Abdul-Wahab, and M. L. Othman, "Solution of optimal power flow using non-dominated sorting multi-objective based hybrid firefly and particle swarm optimization algorithm," *Energies*, vol. 13, no. 16, 2020.

[12] G. Chen, J. Qian, Z. Zhang and Z. Sun, "Applications of novel hybrid bat algorithm with constrained pareto fuzzy dominant rule on multi-objective optimal power flow problems," *IEEE Access*, vol. 7, no. pp. 52060-52084, 2019.

[13] K. Abaci and V. Yamacli, "Differential search algorithm for solving multi-objective optimal power flow problem," *International Journal of Electrical Power & Energy Systems*, vol. 79, pp. 1-10, 2016.

[14] W. Q. Huang, D. B. Chen and R. C. Xu, "A new heuristic algorithm for rectangle packing," *Computers & Operations Research*, vol. 34, no. 11, pp. 3270-3280, 2007.

[15] Z. W. Geem, J. H. Kim and G. V. Loganathan, "A new heuristic optimization algorithm: Harmony search," *Simulation*, vol. 76, no. 2, pp. 60-68, 2001.

[16] W. C. Yeh, "A simple heuristic algorithm for generating all minimal paths," *IEEE Transactions on Reliability*, vol. 56, no. 3, pp. 488-494, 2007.

[17] E. Mesa, J. D. Velasquez and P. Jaramillo, "Evaluation and implementation of heuristic algorithms for non-restricted global optimization," *IEEE Latin America Transactions*, vol. 13, no. 5, pp. 1542-1549, 2015.

[18] X. S. Yang, "Review of meta-heuristics and generalized evolutionary walk algorithm," *International Journal of Bio-Inspired Computation*, vol. 3, no. 2, pp. 77-84, 2011.

[19] J. S. Gero and V. Kazakov, "A genetic engineering approach to genetic algorithms," *Evolutionary Computation*, vol. 9, no. 1, pp. 71-92, 2001.

[20] J. Liu and J. Lampinen, "A fuzzy adaptive differential evolution algorithm," *Soft Computing*, vol. 9, no. 6, pp. 448-462, 2005.

[21] C. H. Martins, R. Dos Santos and F. L. Santos, "Simplified particle swarm optimization algorithm," *Acta Scientiarum-Technology,* vol. 34, no. 1, pp. 21-25, 2012.

[22] F. Hemasian-Etefagh and F. Safi-Esfahani, "Group-based whale optimization algorithm," *Soft Computing*, vol. 24, no. 5, pp. 3647-3673, 2020.

[23] Z. H. Li, Y. H. Li and X. Z. Duan, "Multi-objective optimal reactive power flow using elitist nondominated sorting genetic algorithm: comparison and improvement," *Journal of Electrical Engineering& Technology*, vol. 5, no. 1, pp. 70-78, 2010.

[24] Z. K. Feng, W. J. Niu and C. T. Cheng, "Multi-objective quantum-behaved particle swarm optimization for economic environmental hydrothermal energy system scheduling," *Energy*, vol. 131, pp. 165-178, 2017.

[25] J. G. Hobbie, A. H. Gandomi and I Rahimi, "A Comparison of

Constraint Handling Techniques on NSGA-II," *Archives of Computational Methods in Engineering*, vol. 28, p. 3475-3490, 2021.
[26] H. R. E. H. Bouchekara, A. E. Chaib, M. A. Abido, and R. A. El-Sehiemy, "Optimal power flow using an improved colliding bodies optimization algorithm," *Applied Soft Computing*, vol. 42, pp. 119-131, 2016.
[27] G. Chen, X. Yi, Z. Zhang, and H. Wang, "Applications of multi-objective dimension-based firefly algorithm to optimize the power losses, emission, and cost in power systems," *Applied Soft Computing*, vol. 68, pp. 322-342, 2018.
[28] G. Chen, J. Qian, Z. Zhang, and Z. Sun, "Multi-objective optimal power flow based on hybrid firefly-bat algorithm and constraints-prior object-fuzzy sorting strategy," *IEEE Access*, vol. 7, pp. 139726-139745, 2019.
[29] S. Khunkitti, A. Siritaratiwat and S. Premrudeepreechacharn, "Multi-objective optimal power flow problems based on slime mould algorithm," *Sustainability*, vol. 13, no. 13, 2021.
[30] T. Huy, D. Kim and D. N. Vo, "Multi-objective optimal power flow using multi-objective search group algorithm," *IEEE Access*, vol. 10, pp. 77837-77856, 2022.
[31] S. Chandrasekaran, "Multi-Objective optimal power flow using interior search algorithm: a case study on a real-time electrical network," *Computational Intelligence*, vol. 36, no. 3, pp. 1078-1096, 2020.
[32] S. Khunkitti, A. Siritaratiwat and S. Premrudeepreechacharn, "A many-objective marine predators algorithm for solving many-objective optimal power flow problem," *Applied Sciences-Basel*, vol. 12, no. 22, 2022.
[33] H. T. Kahraman, M. Akbel and S. Duman, "Optimization of optimal power flow problem using multi-objective manta ray foraging optimizer," *Applied Soft Computing*, vol. 116, 2022.
[34] H. Jia, X. Peng and C. Lang, "Remora optimization algorithm," *Expert Systems with Applications*, vol. 185, p. 115665, 2021.
[35] S. Khunkitti, A. Siritaratiwat and S. Premrudeepreechacharn, "Multi-objective optimal power flow problems based on slime mould algorithm," *Sustainability*, vol. 13, no. 13, 2021.
[36] Q Long, G. Q. Li and L Jiang, "A novel solver formulti-objective optimization: dynamic non-dominated sorting genetic algorithm (DNSGA)," *Soft Computing*, vol. 26, p. 725-747, 2022.
[37] J. Q. Zhang, F. Xu and X. W. Fang, "Decomposition of multi-objective evolutionary algorithm based on estimation of distribution," *Applied Mathematics & Information Sciences*, vol. 8, no. 1, pp. 249-254, 2014.
[38] G. Chen, Q. Qin, P. Zhou, P. Kang, X. Zeng, H. Long, and M. Zou, "A Novel Approach Based on Modified and Hybrid Flower Pollination Algorithm to Solve Multi-objective Optimal Power Flow," *IAENG International Journal of Applied Mathematics*, vol. 51, no. 4, pp. 966-983, 2021.
[39] G. Chen, X. Yi, Z. Zhang, and H. Wang, "Applications of multi-objective dimension-based firefly algorithm to optimize the power losses, emission, and cost in power systems," *Applied Soft Computing*, vol. 68, pp. 322-342, 2018.
[40] G. Chen, J. Qian, Z. Zhang and Z. Sun, "Applications of novel hybrid bat algorithm with constrained pareto fuzzy dominant rule on Multi-objective optimal power flow problems," *IEEE Access*, vol. 7, pp. 52060-52084, 2019.
[41] J. Bader and E. Zitzler, "HypE: An algorithm for fast hypervolume-based many-objective optimization," *Evolutionary Computation*, vol. 19, no. 1, pp. 45-76, 2011.